frontiers | Frontiers in Marine Science

TYPE Original Research
PUBLISHED 11 November 2024
DOI 10.3389/fmars.2024.1430572

OPEN ACCESS

EDITED BY
Francisco Javier González,
Instituto Geológico y Minero de España (IGME), Spain

REVIEWED BY
Chunming Dong,
Third Institute of Oceanography, Ministry of Natural Resources, China
Blanca Rincón-Tomás,
Instituto Geológico y Minero de España (IGME), Spain

*CORRESPONDENCE
Qian Liu
liuqian@sio.org.cn

†These authors have contributed equally to this work and share first authorship

RECEIVED 10 May 2024
ACCEPTED 10 October 2024
PUBLISHED 11 November 2024

CITATION
Lai M, Liu Q, Wang X, Sun D, Ran L, Li X, Yang C, Lu B, Xu X-W and Wang C-S (2024) Heterogeneous marine environments diversify microbial-driven polymetallic nodule formation in the South China Sea. *Front. Mar. Sci.* 11:1430572. doi: 10.3389/fmars.2024.1430572

Heterogeneous marine environments diversify microbial-driven polymetallic nodule formation in the South China Sea

Mingyan Lai[1†], Qian Liu[1,2,3*†], Xiaogu Wang[1], Dong Sun[1], Lihua Ran[1], Xiaohu Li[3,4,5], Chenghao Yang[2], Bo Lu[1], Xue-Wei Xu[6] and Chun-Sheng Wang[1,2,5]

[1]Key Laboratory of Marine Ecosystem Dynamics, Second Institute of Oceanography, Ministry of Natural Resources, Hangzhou, China, [2]State Key Laboratory of Satellite Ocean Environment Dynamics, Second Institute of Oceanography, Ministry of Natural Resources, Hangzhou, China, [3]Ocean College, Zhejiang University, Hangzhou, China, [4]Key Laboratory of Submarine Geoscience, Second Institute of Oceanography, Ministry of Natural Resources, Hangzhou, China, [5]School of Oceanography, Shanghai Jiao Tong University, Shanghai, China, [6]National Deep Sea Center, Ministry of Natural Resources, Qingdao, China

Most studies on the genesis of polymetallic nodules suggested that nodules in the South China Sea (SCS) are hydrogenetic; however, the complexity and the heterogeneity in hydrology and geochemistry of the SCS might cause different processes of nodule formation, impacting their application and economic value. Microbial-mediated ferromanganese deposition is an important process in nodule formation, but the related microbial potentials are still unclear in the SCS. In this study, we sampled in three typical regions (A, B, and C) of the SCS enriched with polymetallic nodules. Firstly, we investigated environmental and microbial characteristics of the water columns to determine the heterogeneity of upper seawater that directly influenced deep-sea environments. Then, microbial compositions and structures in sediment cores, overlying waters, and nodules (inside and outside) collected within the same region were analyzed for inferring features of nodule environments. Microbial interactions between nodules and surrounding environments were estimated with collinear network analysis. The microbial evidence indicated that geochemical characteristics in deep sea of the SCS that were key to the polymetallic nodule formation were severely affected by organic matter flux from upper water column. The sediment in region A was sub-oxic due to the large input of terrigenous and phytoplankton-derived organic matter, potentially enhancing the overflow of reduced metals from the porewater. The intense microbial interaction between nodules and surface sediment reinforced the origin of metals for the ferromanganese deposition from the sediment (diagenetic type). Contrarily, the sediments in regions B and C were relatively rich in oxygen, and metal ions could be majorly supplied from seawater (hydrogenetic type). The large discrepancy in microbial communities between nodule inside and remaining samples suggested that nodules experienced a long-term formation process, consistent with the feature of

hydrogenetic nodules. Overall, distributions and interactions of microbial communities in nodules and surrounding environments significantly contributed to the nodule formation in the SCS by manipulating biogeochemical processes that eventually determined the source and the fate of metal ions.

KEYWORDS

polymetallic nodules, The South China Sea, bacteria, archaea, nodule formation

1 Introduction

Polymetallic nodules are important metal sinks in the ocean, tremendously impacting on global ocean metal chemistry (Hein and Koschinsky, 2014; Shiraishi et al., 2016; Chen et al., 2018). They contain rich Mn, Cu, Ni, Co, rare earth elements, and platinum group elements, being considered as economically significant metal sources (Hein et al., 2013, 2015; Hollingsworth et al., 2021). The nodule formation mechanism has been studied since the 1960s (Ehrlich, 1963). Polymetallic nodules usually form at the water–sediment interface, where the sedimentation rate is low (Jiang et al., 2020). They grow slowly (several to hundreds of mm myr^{-1}) via concentric accumulation of iron and manganese oxides around nuclei (Shiraishi et al., 2016; Jiang et al., 2020). Although inorganic processes are often emphasized with respect to the nodule formation, the evidence for the significance of the microbial role in nodule formation is accumulating (Li et al., 2021). Recent studies on micromorphology and microbial community structure reveal microbial contribution to the nodule formation in marine environments; for example, a high abundance of nodule-specific Mn-cycling bacteria (e.g., *Shewanella*, *Colwellia*, and *Pseudoalteromonas*) were identified in nodules from an abyssal plain (Wu et al., 2013; Blöthe et al., 2015), and the microbial communities of the nodules were significantly distinct from the communities in surrounding sediments (Tully and Heidelberg, 2013). These results provide some clues to the biologically driven metal cycle associated with the nodule formation in the seafloor environment.

Generally, polymetallic nodules are classified based on the source of metal ions in the ocean (Chen et al., 2018). A Mn–(Cu +Co+Ni)–Fe ternary diagram is used to divide ferromanganese deposits into three types: hydrogenetic, diagenetic, and hydrothermal types (Halbach et al., 1981). Nodules are solely hydrogenetic when all constituents are derived from seawater (e.g., Cook Islands; Hein et al., 2015) or solely diagenetic when metal ions originate from sediment porewaters (e.g., Peru Basin; von Stackelberg, 2017). Most nodules acquire metals from both sources (Hein and Koschinsky, 2014). Hydrothermal nodules often precipitate in the vicinity of vent sites from fluids with temperatures higher than ambient bottom waters (González et al., 2016). Polymetallic nodules in the Pacific Ocean have been studied extensively with hydrogenetic type in the north-equatorial region and diagenetic type in the east Pacific. Nodules from the Clarion–Clipperton Zone (CCZ) located in the northeast equatorial Pacific Ocean and Central Indian Ocean Basin represent mixed hydrogenetic–diagenetic nodules (Kuhn et al., 2018; Hein et al., 2020), while those from the Peru Basin are mainly diagenetic origin (von Stackelberg, 1997; Zhong et al., 2017).

Marginal seas have been regarded as unfavorable for the formation of ferromanganese nodules, as the large influx of terrigenous sediments can easily dilute Fe and Mn oxides and bury any potential precipitates that may form polymetallic nodules (Zhang et al., 2013). However, the exploration progress in marginal sea shows enriched nodules and crust distributions, such as Galicia Bank at the northwest Atlantic Iberia margin (González et al., 2016), the Gulf of Cadiz (González et al., 2012), the California continental margin (Hein et al., 2005), and Canary Island Seamount Province (Marino et al., 2017), where Fe–Mn deposits are mostly hydrogenetic. As the third largest marginal sea of the world, the investigation of the metallogenic and exploration potentials of polymetallic nodules in the South China Sea (SCS) has been in progress (Zhang et al., 2013; Guan et al., 2017; Zhong et al., 2020; Ren et al., 2023). Increasing detection of Fe–Mn polymetallic deposits in the central basin of the SCS in recent years (Hang and Wang, 2006; Guan et al., 2017, 2019) has suggested that nodules in the SCS are mainly hydrogenetic in terms of the ore composition and the ratio of iron to manganese (Guan et al., 2017; Ren et al., 2023). However, the recognition of nodule types and formation still remains limited in the SCS due to the shortage of nodule exploration and lack of the understanding of microbial contributions. In this study, we selected three typical regions in the SCS where the nodules were ubiquitously distributed and intended to investigate the impact of environmental heterogeneity on geochemical and biological characteristics at the interface of nodules and surrounding environments to understand the mechanisms of polymetallic nodule formation in the SCS. The hypothesized models of the nodule formation were proposed based on the microbial-derived interactions between nodules and surrounding environments.

2 Methods and materials

2.1 Sample collection

The survey was conducted in the SCS during the cruise DY38 by RV Xiangyanghong 9 from 7 April to 13 May in 2017. We sampled at regions A, B, and C where the nodules were detected (Figures 1A, B; Table 1). Region A was located on the edge of the northern slope, and regions B and C were on seamount slopes in the Xisha Sea area and near the Luzon Strait, respectively (Figure 1A). Within each region, seawater samples were collected from discrete depths of the water column at stations CTDA, CTDB, and CTDC using a conductivity–temperature–depth (CTD, SBE 911plus, Sea-Bird Electronics, Bellevue, Washington, US) rosette sampler equipped with 24 10-L sampling bottles (Table 1). Temperature and salinity were monitored with sensors on CTD. The samples for measuring concentrations of particulate organic carbon (POC), dissolved oxygen (DO), chlorophyll-*a* (Chl-*a*), and dissolved inorganic nutrients (NO_3^-, NO_2^-, and NH_4^+) in the water column were collected on board and analyzed following the standard methods for the specification for marine monitoring (GB 17378-2007). Briefly, DO concentrations in seawater were measured with the Winkler titration method onboard. Water samples (~1 L) for the analysis of Chl-*a* were filtered on 47 mm Whatman GF/C glass fiber filters, and Chl-*a* was extracted into 90% acetone and measured with a Trilogy Laboratory Fluorometer. Approximately 100-mL filtrates were frozen at −20°C for each sample, and [NO_3^-], [NO_2^-], and [NH_4^+] were determined by SmartChem® 600 Automated Discrete Analyzer (KPM Analytics located in Westborough, MA, USA) in the laboratory. Approximately 5 L water was filtered on precombusted Whatman GF/F filter for POC concentration measurement. The filters were frozen at -20°C until analysis. In the laboratory, the filters were dried at 50°C for 48 h and fumigated using HCl (12 mol/L) for 24 h. They were washed by Milli-Q water, dried at 50°C for 48 h, and measured with an elemental analyzer (Flash EA 2000, Thermo Fisher Scientific, Lenexa, KS, USA).

Meanwhile, we selected typical depths (surface, depth of Chl-*a* maximum, bottom of epipelagic zone, mesopelagic zone, oxygen minimum zone, bathypelagic layer, and near bottom depth) for microbial community analysis (Table 1). A total of 5 L of seawater was filtered through 0.22-μm pore size filters, which were stored at −80°C onboard until subsequent analysis. Polymetallic nodules (n=11), sediment column (0–22 cm; n=33), and ~150 ml of overlying water (n=5) of the surface sediment were aseptically sampled from pushcores using the manned submersible "Jiaolong" during dives A–C in regions A–C, respectively

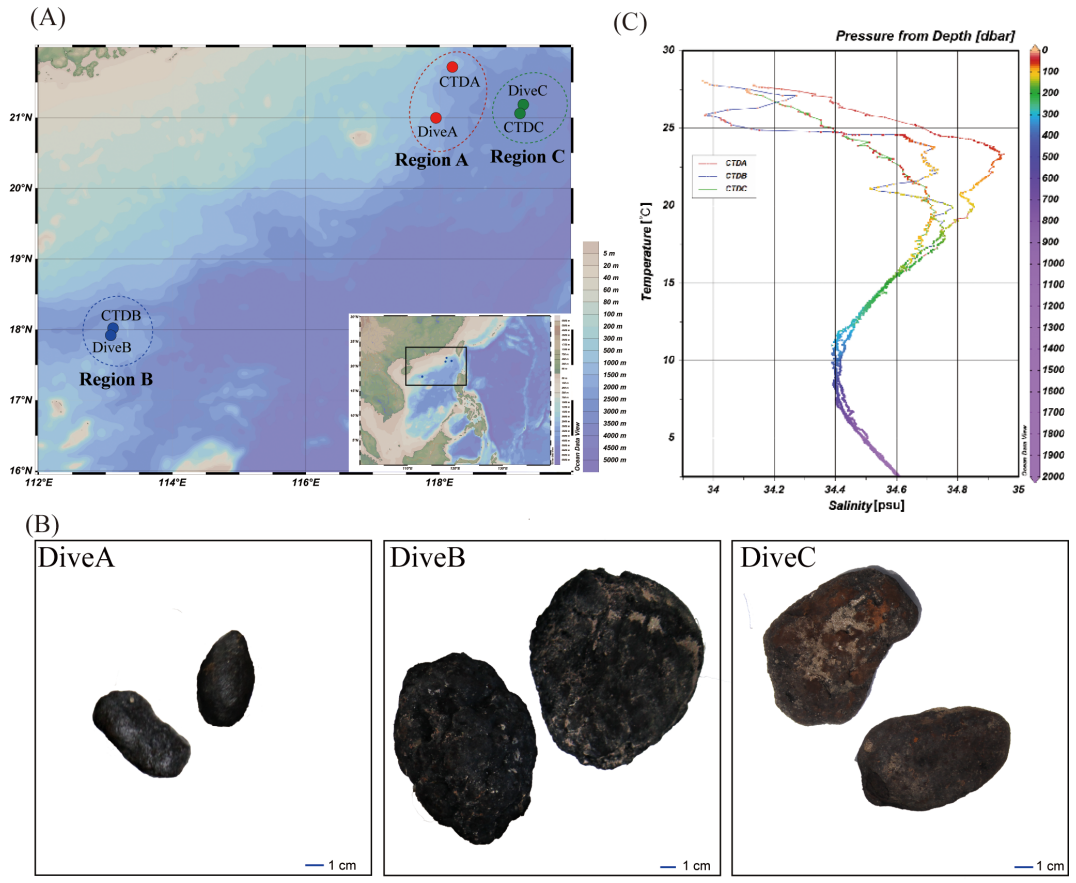

FIGURE 1
Study regions and specific sampling sites in the South China Sea (SCS). **(A)** A map showing the sampling areas of the SCS, including region A (CTDA and DiveA), region B (CTDB and DiveB), and region C (CTDC and DiveC); **(B)** nodules sampled from different dives in the SCS; **(C)** temperature (°C)–salinity diagram (T–S) from all CTD stations in the SCS.

(Table 1; Supplementary Figure 1). On board, a series of sample operations were conducted after removing the samples from the push core. The nodules were gently cleaned with aseptic waters, and small portions (approximately 0.5 g) of surface and interior samples were collected using a sterile chisel and hammer. Sediment samples were sectioned at an interval of 2 cm. Nodule and sediment samples were sealed individually in axenic bags. The overlying water was processed by the same approach as the seawater sample. All samples were stored at −80°C for microbial analyses.

2.2 DNA extraction, PCR amplification, and Illumina sequencing of 16S rRNA genes

DNA was extracted from filtered water samples, 0.5 g of nodules, and sediment samples (n=68; Table 1) with the Fast DNA™ SPIN Kit for Soil (MP Bio, Carlsbad, CA, USA) following the steps recommended by the manufacture, including the bead-beating for additional cell disruption prior to the extraction in nodule and sediment samples (Lindh et al., 2017; Shulse et al., 2017). The DNA concentration and quality were assessed using a NanoDrop ND-2000c Spectrophotometer (Thermo Scientific, Inc., USA). Extracted DNA was stored at − 80°C for downstream sequencing.

The V3–V5 hypervariable regions of archaeal 16S rRNA genes were amplified by the primer pair Arch344F (ACGGGGYGCAGCAGGCGCGA)/Arch915R (GTGCTCCCCCGCCAATTCCT) (Zheng et al., 2013), and the primer pair of 338F (5′-ACTCCTACGGGAGGCAGCA-3′)/806R (5′-GGACTACHVGGGTWTCTAAT-3′) was used to amplify the V3–V4 region of bacterial 16S rRNA genes (Caporaso et al., 2011). The amplicon processing was performed as described in Liu et al. (2023). Negative (no sample) extraction controls were used for PCR amplification to check for the presence of possible environmental contamination (Sheik et al., 2018). Pair-end sequencing was carried out by the Illumina Miseq PE250 platform (Majorbio Bio-Pharm Technology, Shanghai, China).

2.3 Data analysis

Trimmomatic (Bolger et al., 2014) was used for the quality control of raw reads following the criteria reported previously (Liu et al., 2020). Operational taxonomic units (OTUs) were clustered in UPARSE (Edgar, 2013) at a 97% similarity cutoff and taxonomically assigned with the Ribosomal Database Project (RDP) naive–Bayersian classifier against the Silva database Release 138 (http://www.arb-silva.de). A total of 2,684,460 bacterial 16S rRNA gene sequences were obtained from 66 samples and 2,875,089 archaeal sequences from 67 samples (Supplementary Table S1). Specifically, 1,826 bacterial OTUs and 946 archaeal OTUs were recovered from 817,233 bacterial sequences (417 bp average length) and 953,783 archaeal sequences (265 bp average length) of 18 water column samples, respectively, and 6,371 bacterial OTUs and 4254 archaeal OTUs were identified from 1,867,727 bacterial sequences (434 bp average length) and 1,921,306 archaeal sequences (335 bp average length) from samples of sediment, nodules, and overlying water. The rarefaction curves for the observed OTUs from bacteria and archaea showed clear asymptotes (Supplementary Figure S2), indicating a near-complete sampling of the community. OTUs affiliated with chloroplasts and eukaryotes were removed from

TABLE 1 The geographic information of sampling sites in the South China Sea.

Regions	Stations	Longitude (°E)	Latitude (°N)	Total water depth (m)	Sample types	Sampling depths/names
A	CTDA	118.17	21.73	1,304	seawater	0, 10*, 30, 50*, 75, 100*, 125, 150, 200*, 300, 500*, 800, 1000, 1303* m
	DiveA	117.95	20.98	1,397	overlying water	DiveA_OW1; DiveA_OW2
					sediment	0-22 cm b.s.f.
					nodule	DiveA_NO1, DiveA_NO2, DiveA_NO3, DiveA_NI
B	CTDB	113.09	17.96	1,957	seawater	0, 2*, 10, 30*, 50, 85*, 100, 125, 150, 200*, 300, 500, 800*, 1000*, 1500, 1977* m
	DiveB	113.07	17.89	1,733	overlying water	DiveB_OW
					sediment	0-22 cm b.s.f.
					nodule	DiveB_NO1, DiveB_NO2, DiveB_NI1, DiveB_NI2
C	CTDC	119.23	21.09	1,617	seawater	0, 10, 30, 50*, 75, 100*, 125, 150, 200*, 300, 500, 800*, 1100, 1500, 1616* m
	DiveC	119.24	21.14	1,773	overlying water	DiveC_OW1, DiveC_OW2
					sediment	0-22 cm b.s.f.
					nodule	DiveC_NO1, DiveC_NO2, DiveC_NI

*Water samples were selected for microbial analysis.

subsequent analyses. Sequencing depths of water column samples were standardized to 28,429 reads for bacteria and 24,682 reads for archaea. The sequencing depth was normalized to 4,684 reads for the bacterial sample collected from 1,977 m of CTDB due to the low number of reads (Supplementary Table S1); however, since the curve of this sample on the rarefaction curve still showed a clear asymptote (Supplementary Figure S1), the sample was included in the analysis. The sequencing depth of each sample was equalized to 22,351 reads in bacteria and 18,195 reads in archaea corresponding to the lowest sequence number among sediment, nodule, and overlying water samples. The OTU tables were normalized by dividing the number of sequences for each OTU by the total number of sequences in each sample, i.e., normalization to relative abundances. The results of relative abundance were visualized in TBtools (version 0.1098765) software (Chen et al., 2020). Statistical data processing was performed using the Origin 2022 and R (RStudio) 3.6.0 (Kronthaler and Zöllner, 2021).

Based on taxonomic information, statistical analysis of community structure was performed at various taxonomic levels. Alpha-diversity metrics (i.e., Shannon and Chao1 indices) were calculated based on OTU relative abundances for each sample. Beta-diversity across samples was analyzed using the Bray–Curtis distance matrix and visualized using non-metric multidimensional scaling (NMDS, package Phyloseq) and hierarchical clustering tree. Nonparametric analysis of similarities (ANOSIM) was performed on Bray–Curtis community dissimilarities in the R package vegan (Anderson, 2006). Similarity percentage (SIMPER) in PRIMER package V6.0 (Primer-E, UK) was used to identify the taxa that contributed to the dissimilarity between groups (Clarke and Gorley, 2006). The difference in the diversity indices of microbial groups among different samples were analyzed by Kruskal–Wallis H test, and the significant level of the difference (p-value) was evaluated.

We performed collinear network analysis using the NetworkX software (version1.11; Hagberg et al., 2008) based on bacterial and archaeal OTUs, respectively, to identify the interaction of four sample types (nodule outside, nodule inside, surface sediment, and overlying water) and key species at interfacial layers of nodules and surrounding environments. The networks were composed of interconnected nodes, representing the sample node and the species node, and the connection between these two nodes indicated the inclusion of the species in the sample. The number of connections from a node is called the degree of the node. Degree centrality, betweenness centrality, and closeness centrality were studied to obtain the information contained in the network. Degree centrality was measured as the number of direct links that involved a given node (Yuan et al., 2011), and the higher value meant that the node was more central. Closeness centrality is the shortest path between a node and all other reachable nodes (Bröhl and Lehnertz, 2022). Betweenness centrality is a measure of centrality of a node that acts as a bridge along the shortest path between two other nodes (Wasserman and Faust, 1994). Directed networks visualizing the OTU distribution in different samples were generated using the preferred layout algorithm in CYTOSCAPE 3.0 (Shannon et al., 2003).

3 Results

3.1 Environmental characteristics of the water column

The temperature–salinity (T–S) diagram revealed that the upper water masses (<200 m) of stations CTDA, CTDB, and CTDC exhibited different characteristics, while the deep water was relatively homogeneous across all stations (Figure 1C). The water columns of stations CTDA and CTDC exhibited well-developed surface mixed layers (SML) above 16 m and 12 m, respectively, while SML at Sta CTDB was not obvious, approximately at 26 m (Supplementary Figures S3A, B). Nitrate concentrations were below detection limit above 50 m, 75 m, and 25 m at stations CTDA, CTDB, and CTDC, respectively (Figure 2A). The depth of the Chl-*a* maximum (DCM) at Sta CTDB (~85 m) was deeper than that at other two stations (~50 m), and the maximum Chl-*a* concentration (CTDB: 0.45 μg/L) was lower (CTDA: 1.13 μg/L, CTDC: 1.10 μg/L; Figure 2B). The peak of POC concentrations in the water column was in correspondence to that of Chl-*a* except at Sta CTDB, where the highest POC concentration was in surface water. The second peak of POC concentration at Sta CTDA occurred in surface water as well (Figure 2C). The oxygen minimum zone (OMZ) ranged from 800 to 1,000 m at three stations, and stations CTDA and CTDC had a relatively narrow OMZ in comparison to that at Sta CTDB (Figure 2D).

3.2 Microbial community composition and diversity in the water columns

The profiles of Shannon and Chao1 indices showed that the variations in bacterial and archaeal diversity and richness in the water column were similar at stations CTDA and CTDC, while those at Sta CTDB were relatively higher below 200 m (Supplementary Figures S4A, B). The NMDS analyses showed that bacterial and archaeal communities in water column samples of three stations were clearly divided into different groups (Figure 3). The bacterial communities above 100 m were clustered together, while those below 200 m at Sta CTDB were distinctively separated from other two stations (Figure 3A). The archaeal communities from 100 m to 200 m and deep water of three stations (500–1,977 m) were separated except that at 800 m of Sta CTDB (Figure 3B).

A majority of the classified bacterial sequences in water columns of three stations were assigned to Proteobacteria (598 OTUs, 60.9% of total bacterial sequences), followed by Cyanobacteria (9 OTUs, 14.8%), Actinobacteriota (58 OTUs, 5.2%), SAR406 clade (112 OTUs, 4.1%), and Bacteroidota (155 OTUs, 3.5%) (Figures 3A; Supplementary Figure S5). The dominant bacterial groups varied at different depths (Figure 3A). Cyanobacteria were most abundant above the DCM layer (53.3 ± 8.7%), and more than 97% belonged to *Prochlorococcus* MIT9313 and *Synechococcus* CC9902 (Figure 3A). Below the DCM layer, Proteobacteria became dominant, especially at

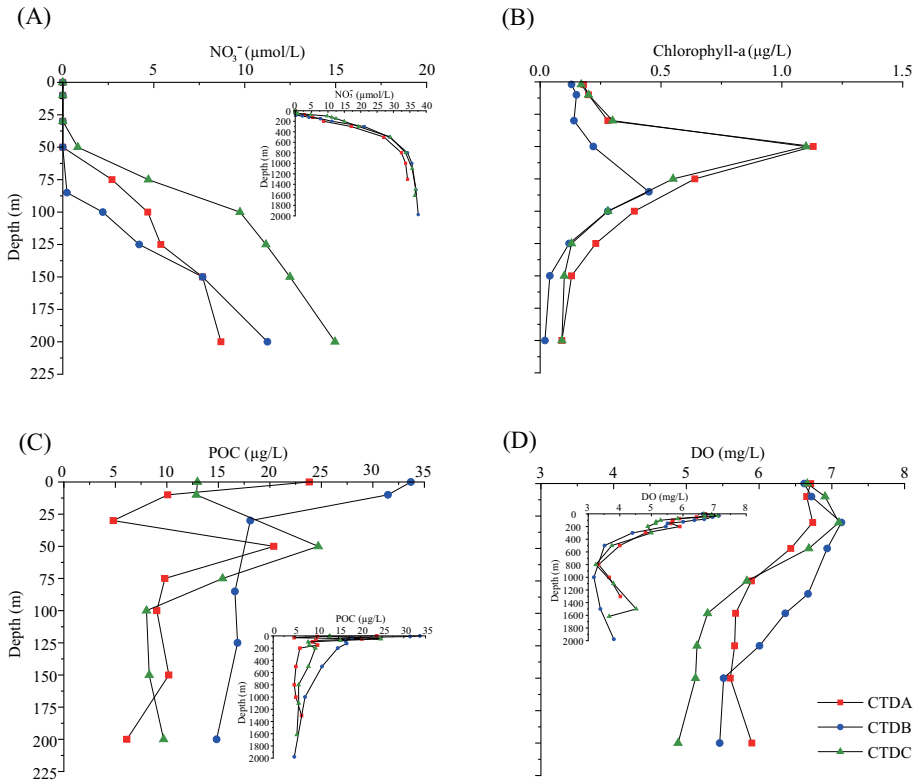

FIGURE 2
The concentrations of **(A)** nitrate, **(B)** chlorophyll *a*, **(C)** particulate organic carbon (POC), and **(D)** dissolve oxygen (DO) in the water column samples of stations CTDA, CTDB, and CTDC in the South China Sea.

stations CTDA and CTDC (>85%), but the composition was different (Figure 3A). *Alteromonas* was the most abundant genus (>45% of Proteobacteria) at 50 m of Sta CTDA, and *Alcanivorax* (25.6 ± 16.3%) and *Marinobacter* (20.3 ± 13.7%) were dominant at depths of 200–1,303 m. At Sta CTDC, a higher proportion of *Salinicola* (20.2 ± 12.7%) was detected below 200 m (Figure 3A). The SIMPER analysis confirmed that *Marinobacter*, *Alcanivorax*, and *Salinicola* contributed to the difference in microbial communities below 200 m between stations CTDA and CTDC (Supplementary Table S2). At Sta CTDB, the relative abundances of the phyla SAR406 clade and SAR324 clade exceeded 10% of total bacterial sequences below 200 m (Figure 3A). The major groups contributing to the difference in bacterial communities below 200 m between CTDB and other two stations included SAR324 clade, SAR406 clade, SAR202 clade, *Marinobacter*, and Sva0996 marine group (Supplementary Table S2).

The archaeal communities were mainly assigned to the phyla Thermoplasmatota and Thaumarchaeota (Figure 3B). Marine group II (MGII) and marine group III (MGIII) of *Thermoplasmatota* were dominant (>50%) through the water column of all stations except 800 m at Sta CTDB (Figure 3B). The relative abundance of Thaumarchaeota increased from 50 m and occupied 29.8 ± 7.5% of total archaeal sequences below 200 m (Figure 3B). *Candidatus* Nitrosopelagicus dominated above 200 m (14.0 ± 10.6%), while the relative abundance of unclassified genera in Nitrosopumilaceae increased below 200 m (CTDA: 18.1 ± 7.3%, CTDB: 31.8 ± 7.9%, CTDC: 18.1 ± 8.1%; Figure 3B). Although there was little variation in archaeal communities in deep water layers (≥200 m) among three stations compared to that of bacterial community (ANOSIM, bacteria: R=0.6212, p-value=0.008; archaea: R=−0.1566, p-value=0.836; Figure 3), the dissimilarity of archaeal community between CTDB and other two stations below 200 m were larger (CTDB vs. CTDA: 30.4%; CTDB vs. CTDC: 29.6%) than that between stations CTDA and CTDC (16.4%; Supplementary Table S2). MGII and MGIII that were relatively more abundant at stations CTDA and CTDC contributed to over 40% of the difference, followed by family Nitrosopumilaceae (~23%) and a group of unidentified archaea (Supplementary Table S2).

3.3 Microbial community composition and diversity in the sediment cores

The bacterial Shannon and Chao1 indices decreased from the surface of three sediment cores collected from DiveA, DiveB, and DiveC (Supplementary Figure S4C), while those of archaea had an opposite trend with a fluctuation below 6 cm (Supplementary Figure S4D). The hierarchical clustering based on Bray–Curtis distance estimation at OTU level showed that the bacterial communities in sediment cores of all dives were divided into three clusters (similarity within each cluster >70%; Supplementary Figure S6A). Cluster I included bacterial communities at depths of 0–2 cm of DiveA, 0–12

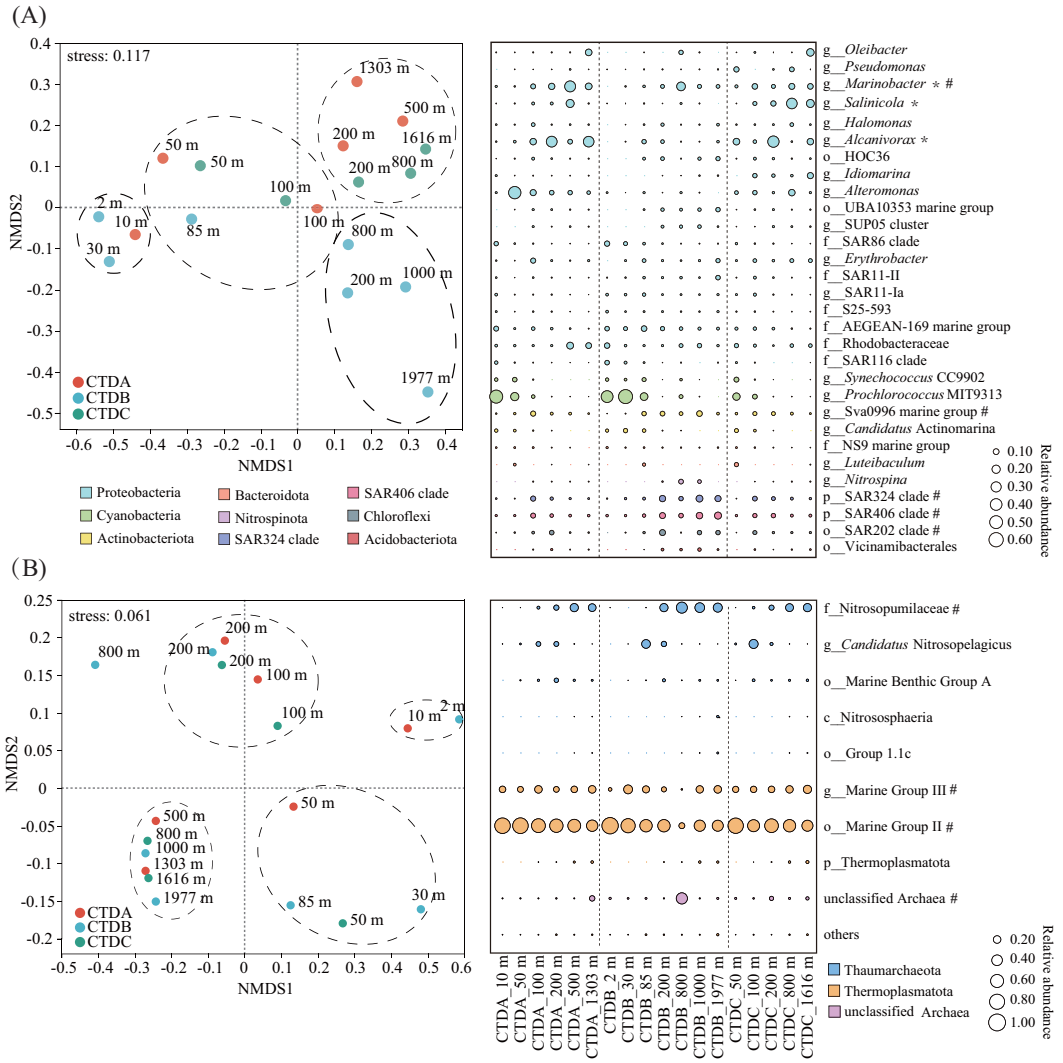

FIGURE 3
Characteristics of microbial communities in water column samples of stations CTDA, CTDB, and CTDC in the South China Sea. **(A)** The NMDS analysis of bacterial community and top 30 bacterial taxa; **(B)** the NMDS analysis of archaeal community and the dominant archaeal taxa (relative abundance>1%). The asterisk and hashtag indicated groups that contributed to differences between microbial communities in water column samples of stations CTDA and CTDC and between those of Sta CTDB and other two stations below 200 m. The black circles in NMDS analyses differentiated the clusters of bacterial and archaeal communities in water column samples of three stations.

cm of DiveB, and 0–6 cm of DiveC. Cluster II was composed of those at 6–22 cm of DiveC, and the remaining ones of DiveA and DiveB were grouped into Cluster III (Supplementary Figure S6A). It also revealed that the bacterial communities in Clusters I and II were closely related (Supplementary Figure S6A). The archaeal community in sediment samples followed a similar pattern of clustering, but it was noted that the archaeal community at 2–4 cm of DiveA was grouped with that at 0–2 cm of the same dive (Supplementary Figure S6B).

The dominant bacterial communities (>3% of total bacterial sequences) in sediment cores were composed of the phyla Chloroflexi (28.1%), Proteobacteria (23%), Acidobacteriota (9.5%), Actinobacteriota (6.1%), Methylomirabilota (4.3%), NB1-j (3.9%), Gemmatimonadota (3.6%), and Planctomycetota (3.4%; Figure 4A). The transition from Cluster I to Cluster III occurred clearly at 2 cm and 12 cm of DiveA and DiveB, respectively (Figure 4A). Most genera from Chloroflexi, such as the unclassified genera from the order S085, family Anaerolineaceae, classes Dehalococcoidia, and JG30-KF-CM66, were mainly distributed in sediments below the transition layer, contributing 28.2% to the difference between Clusters I and III (Figure 4; Supplementary Table S3). Several genera of Proteobacteria also led to more than 15% of the difference (Figure 4B; Supplementary Table S3); for example, a decline in relative abundances of *Woeseia*, *AqS1*, and unclassified genera from family Kiloniellaceae, orders MBMPE27, JTB23, and AT-s2-59, were observed with the increase of the depth (Figure 4A). The genus *Nitrospira* and the phylum NB1-j showed a similar pattern to most Proteobacteria groups and contributed ~8% to the difference between Clusters I and III (Figure 4; Supplementary Table S3). The unclassified genera belonging to the order Aminicenantales of the phylum Acidobacteriota were only present in Cluster III (Figure 4). Other Acidobacteriota, such as the classes Subgroup 21 and Subgroup 22,

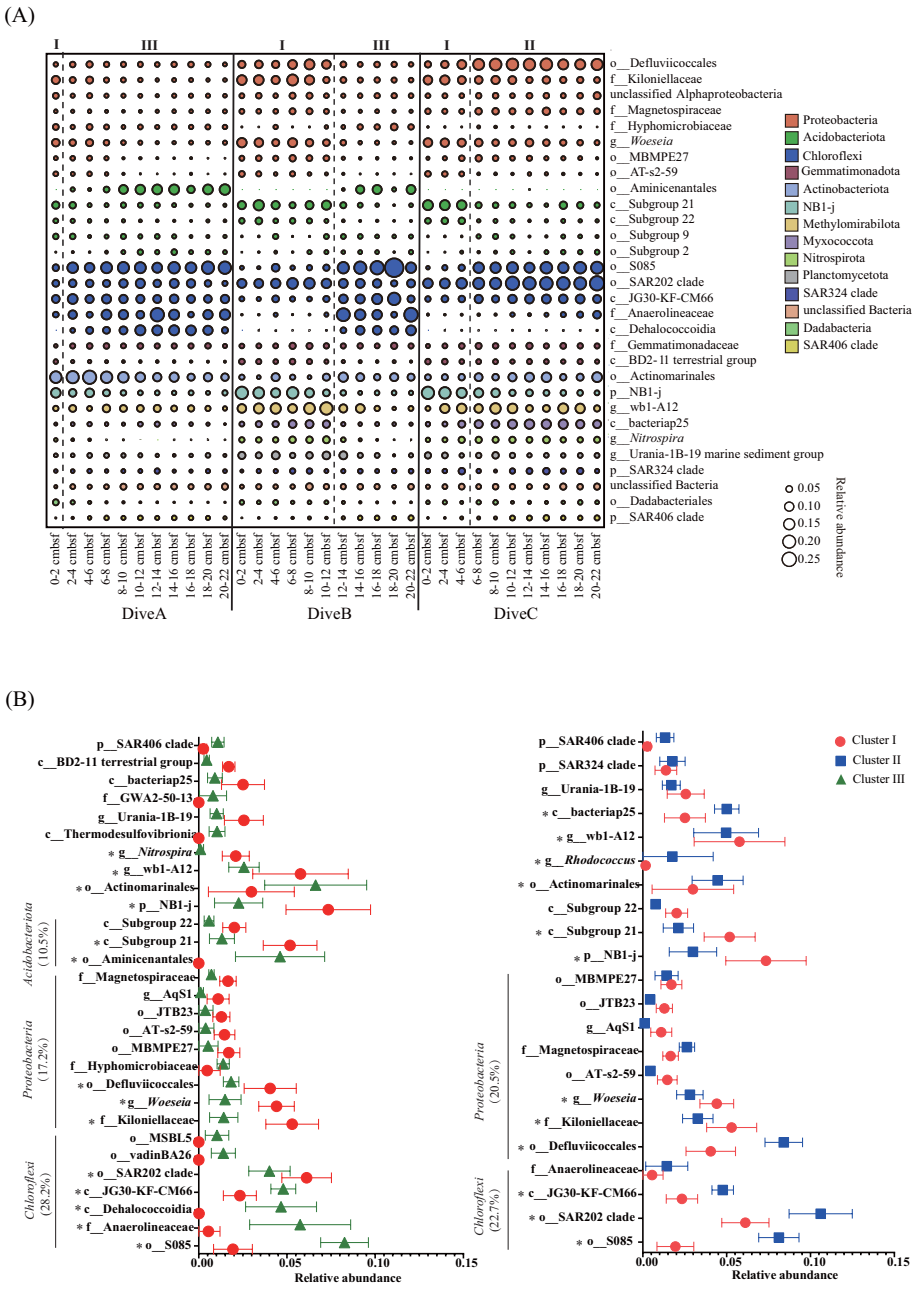

FIGURE 4
Characteristics of bacterial communities in sediment cores of DiveA, DiveB, and DiveC in the South China Sea. **(A)** The distribution of top 30 bacterial taxa in sediment cores of DiveA, DiveB, and DiveC; **(B)** the comparisons of the means of relative abundances of bacterial taxa between Cluster I and Cluster III, and between Cluster I and Cluster II based on β-diversity analysis of bacterial communities shown in Supplementary Figure S6. The asterisks highlighted the taxon that contributed over 2% to the dissimilarity of the bacterial community between two clusters by referring to Supplementary Table S3.

decreased in relative abundances with the increasing depth (Figure 4A). The three groups of Acidobacteriota contributed 10.5% to the difference between Clusters I and III (Figure 4B). Genera from phylum Desulfobacterota, a low-prevalence taxon, were enriched in Cluster III (Supplementary Figure S7). The transition of bacterial community from Cluster I to Cluster II only occurred at 6 cm in DiveC (Supplementary Figure S6A; Figure 4A). The dissimilarity of the bacterial community between Clusters I and II (36.0%) were low in comparison to those between Clusters I and III (55.1%) and Clusters II and III (44.4%; Supplementary Table S3). The genera belonging to the orders Defluviicoccales, S08, SAR202 clade and the class bacteriap25 were enriched at 6–22 cm of DiveC (Cluster II), which contributed more than 18% to the difference between Clusters I and II (SIMPER analysis; Figure 4; Supplementary Table S3).

Thaumarchaeota was the most abundant archaeal group in sediment cores from DiveA, DiveB, and DiveC, and the genera composing Thaumarchaeota showed different distribution patterns among dives (Figure 5). Unidentified genera in family

Nitrosopumilaceae were widely distributed in Clusters I and II (Figure 5A). *Ca.* Nitrosopumilus and *Ca.* Nitrosopelagicus were relatively abundant in Cluster I and sharply declined or disappeared in Clusters II and III (Figure 5). In contrary, Marine Benthic Group A was mainly distributed in Cluster III (Figure 5). The family Nitrosopumilaceae, Marine Benthic Group A, and *Ca.* Nitrosopumilus contributed ~61.5% to the difference between Clusters I and III, while the rest (20.1%) were mainly received from the family Geothermarchaeaceae, classes Lokiarchaeia and Bathyarchaeia, and the order Hydrothermarchaeales, which were mainly present in Cluster III (Figure 5B; Supplementary Table S3). The distinct division between Clusters I and II occurred in DiveC, but again, the dissimilarity was relatively low (36.3%; Supplementary Table S3). The Simper analysis showed that the major groups contributing to the difference (a total of 74.2%) were *Ca.* Nitrosopumilus, the family Nitrosopumilaceae, the order Woesearchaeales, and the class Deep Sea Euryarchaeotic Group (DSEG; Figure 5B; Supplementary Table S3).

3.4 Comparison of microbial communities in polymetallic nodules with surrounding environments

The Shannon indices of bacterial communities in nodules were not different from those in surface sediments (SS) and overlying waters (OW; Kruskal–Wallis H test and *post-hoc* Dunn's test, *p*-value>0.05), but the archaeal community in nodules showed a lower

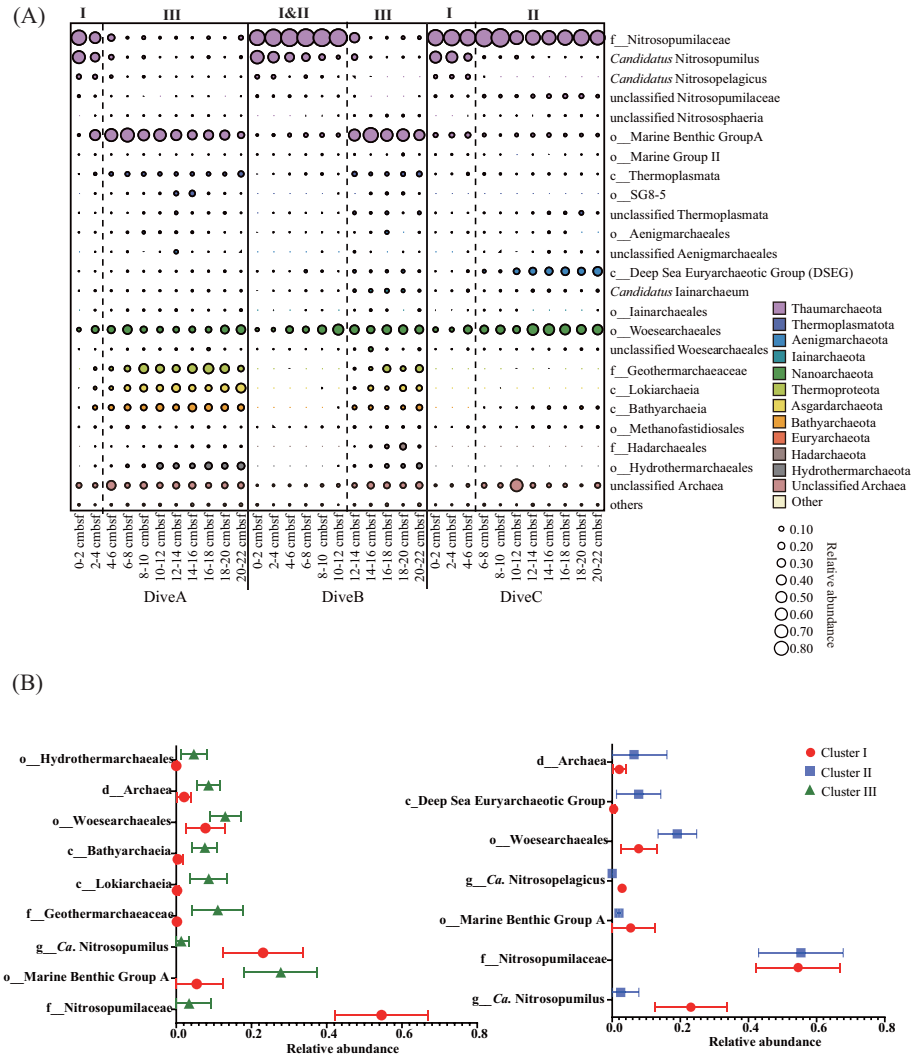

FIGURE 5
Characteristics of archaeal communities in sediment cores of DiveA, DiveB, and DiveC in the South China Sea **(A)** The distribution of the dominant archaeal taxa (relative abundance >1%) in sediment cores of DiveA, DiveB, and DiveC; **(B)** the comparisons of the means of relative abundances of archaeal taxa between Cluster I and Cluster III and between Cluster I and Cluster II based on β-diversity analysis of archaeal communities shown in Supplementary Figure S6. The asterisks highlighted the taxon that contributed over 2% to the dissimilarity of the archaeal community between two clusters by referring to Supplementary Table S3.

index than that in OW (p-value<0.05). The Chao1 index of the microbial community showed a distinctive variation between nodules and surrounding environments. Bacterial Chao1 indices of NO and NI samples were much lower than that of SS, while the archaeal Chao1 index of NI was lower than those of SS and OW (p-value<0.05). There was no significant difference in bacterial or archaeal Shannon and Chao1 indices between samples of nodule outside (NO) and inside (NI; Supplementary Figures S8A, B). There was a relatively large discrepancy in bacterial communities of OW or NI samples among different dives, while the archaeal community showed large discrepancies in all samples of NO or NI. The microbial communities in SS samples varied rarely among samples (Supplementary Figure S8C). The distance calculated at OTU level among different sample groups (shown by "between") were relatively higher than that within each sample group (ANOSIM; bacteria: R=0.8067, p-value=0.001; archaea: R=0.6462, p-value=0.001; Supplementary Figure S8C). The NMDS analysis also revealed that the sample type was the primary control of microbial community composition in the SCS (Figure 6). Microbial communities at OTU level in nodule samples (NO and NI) were separated from those in SS and OW (Figure 6). The number and the proportion of bacterial or archaeal OTUs shared by

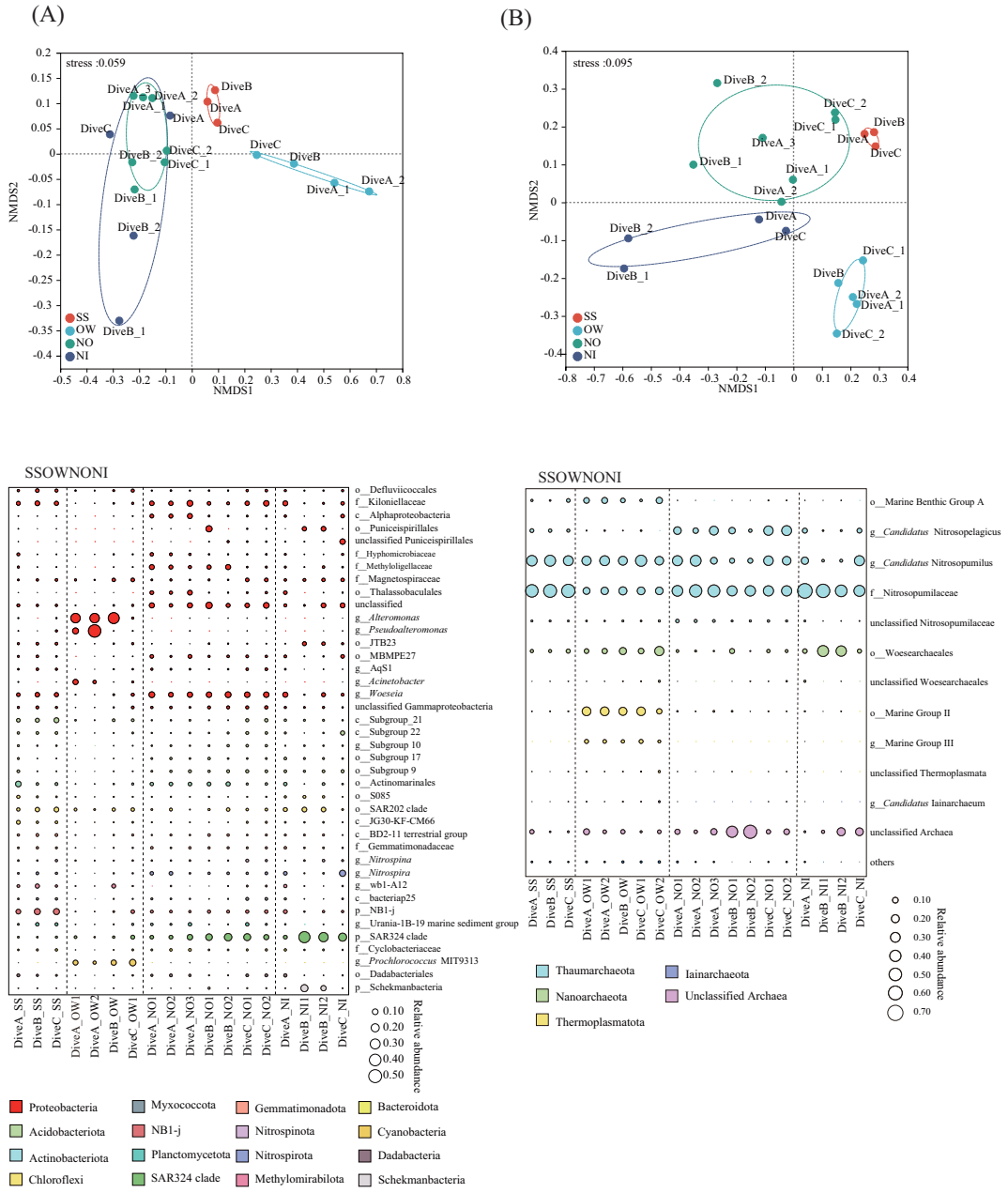

FIGURE 6
Characteristics of microbial communities in samples of surface sediment (SS), overlying water (OW), and nodules (NO, nodule outside; NI, nodule inside). **(A)** The NMDS analysis and top 30 bacterial taxa of the bacterial community; **(B)** the NMDS analysis and the dominant archaeal taxa (relative abundance >1%) of the archaeal community.

10.3389/fmars.2024.1430572

nodules and surrounding environments (OW and SS) or either one were highest in samples of DiveA (Supplementary Figure S9).

SAR324 clade was the dominant group in all nodule samples, especially at DiveB and DiveC (Figure 6A). The Proteobacteria linages showed an enrichment in NO samples. The genus *Woeseia* and the family Kiloniellaceae, which were abundant in SS, were also dominant in NO of all dives and NI of DiveA (Figure 6A). The family Hyphomicrobiaceae was shared by samples of NO and SS of DiveA (Figure 6A). Bacterial communities in OW were dominated by the phyla Proteobacteria and Cyanobacteria, representing over 60% of bacterial sequences. *Prochlorococcus* MIT9313 was the most dominant cyanobacterial group, mainly distributed in OW of DiveC and DiveB (Figure 6A). *Alteromonas* of Proteobacteria was enriched at DiveA and DiveB, while *Pseudoalteromonas* occupied abundantly only in OW of DiveA. The dominant genera *Halomonas*, *Pseudoalteromonas*, *Acinetobacter*, *Oleibacter*, and *Marinobacter* in OW of DiveA were relatively low in nodule and SS samples (Figure 6A; Supplementary Figure S10). Taxa from family Magnetospiraceae were mainly distributed in OW and nodules of DiveC, and OW and NI of DiveB (Figure 6A).

Thaumarchaeota was also a major group in nodule samples that both *Ca.* Nitrosopelagicus and *Ca.* Nitrosopumilus were enriched in nodules of DiveA and DiveC. At DiveB, the order *Woesearchaeale* in the phylum *Nanoarchaeotas* were relatively abundant in NI (Figure 6B). In addition, it was noteworthy that a large number of unidentified archaea were found in nodule samples of DiveB (Figure 6B). The archaeal communities in OW were similar among different dives and dominated by Thaumarchaeota, Thermoplasmatota, and Nanoarchaeota (Figure 6B). Marine Benthic Group A of Thaumarchaeota and MGII and MGIII of Thermoplasmatota were almost exclusively distributed in OW (Figure 6B).

3.5 Collinear network analysis of microbial communities from polymetallic nodules and surrounding environments

The collinear network was performed at bacterial OTU level with all samples (SS, OW, NO, and NI) for each dive (Figure 7). The network contained 3,361 effective nodes in DiveA, more than those in DiveB (3,021) and DiveC (3,164). The network centralization was 0.647, 0.624, and 0.653 in networks of DiveA, DiveB, and DiveC, respectively. In DiveA, the SS sample had 2,175 degrees, followed by samples of NO (1,589), NI (1,382), and OW (1,252; Supplementary Table S4). Similarly, the values of degree centrality, betweenness centrality, and closeness centrality were highest in samples of SS and NO (Supplementary Table S4). There were 63 dominant OTUs (after the filtration with the total OTU abundance at one station >200) that had the highest centrality measurement, most of which were prevalent in both SS and nodule samples, such as OTUs identified as the class Subgroup 21; the orders Subgroup 17, MBMPE27, and Actinomarinales; the families Hyphomicrobiaceae, Kiloniellaceae, and Methyloligellaceae; and the genera *Woeseia*, wb1-A12, *Nitrospira*, and AqS1 (Supplementary Table S5). In networks of DiveB and DiveC, the highest degree was also found in SS samples,

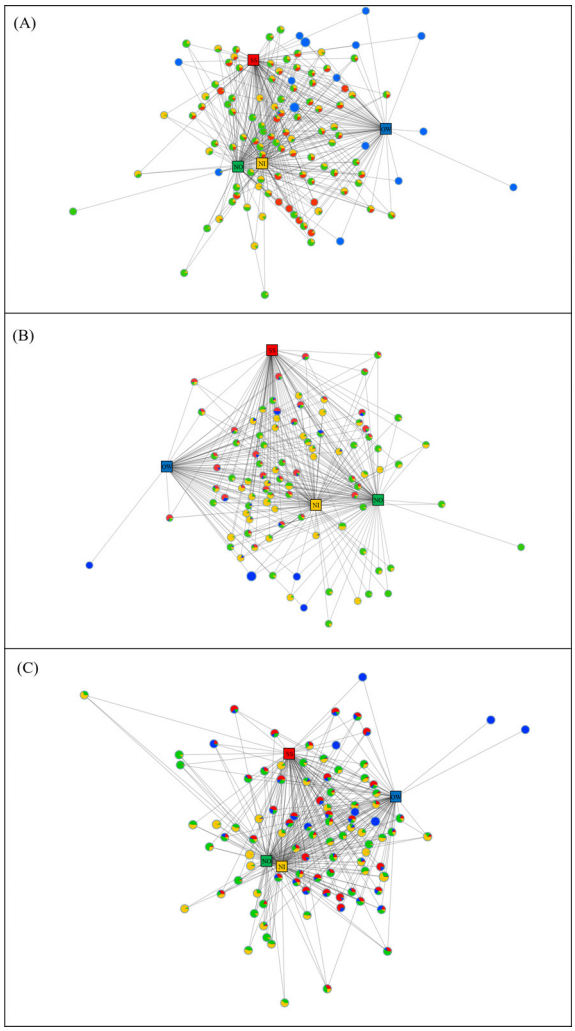

FIGURE 7
Collinear network analysis at bacterial OTU level on samples of surface sediment (SS), overlying water (OW), and nodules (NO, nodule outside; NI, nodule inside) for **(A)** DiveA, **(B)** DiveB, and **(C)** DiveC. Networks were analyzed based on all OTUs of each dive, but only those with the number beyond 200 were displayed. The square nodes represent sample types (red, SS; blue, OW; green, NO; yellow, NI) as source nodes, and the circle nodes are key OTUs as target nodes. The proportion of colors in the circle means the relative abundances of the OTU in the corresponding sources.

but the degree of OW exceeded those of nodules (Supplementary Tables S6, S7). Degree centrality, betweenness centrality, and closeness centrality exhibited similar trends (Supplementary Table S4). The numbers of dominant OTUs characterized by the highest centrality were 65 and 67 in networks of DiveB and DiveC, respectively (Supplementary Tables S6, S7). In DiveB, the taxa belonging to the class Subgroup 21 and the genus wb1-A12 were the key species mostly abundant in SS and OW. The classes BD2-11 terrestrial group and Gammaproteobacteria, the orders Actinomarinales and MBMPE27, the family Magnetospiraceae, and the genera Woeseia and Nitrospira were enriched in both SS and nodule samples (Supplementary Table S6). Few OTUs occurred in large numbers in nodules and OW simultaneously (Supplementary Figure S9; Supplementary Table S6). OTU from the family Hyphomicrobiaceae were mainly distributed in

OW and NO (Supplementary Table S6). In DiveC, NO, SS, and OW shared more OTUs compared to other dives, including those belonging to the classes Subgroup 21, Gammaproteobacteria, and BD2-11 terrestrial group, and the genera *Woeseia* and AqS1 (Supplementary Figure S9; Supplementary Table S7). The order MBMPE27, the families Magnetospiraceae and Kiloniellaceae, and the genera *Woeseia* and *Nitrospira* were prevalent in SS and nodule samples (Supplementary Table S7).

The numbers of effective nodes of the collinear networks based on archaeal OTUs were 1,379, 1,490, and B8 in DiveA, DiveB, and DiveC, respectively, with the network centralization of 0.632, 0.584, and 0.447 (Supplementary Figure S11). Both degree and centrality measurements of OW were highest among samples for each dive, followed by SS (DiveA) or NO (DiveB and DiveC; Supplementary Table S4). The dominant OTUs with highest centrality measurements (DiveA: 44 OTUs, DiveB: 35 OTUs, and DiveC: 32 OTUs) majorly belonged to the orders MGII and Marine Benthic Group A, family Nitrosopumilaceae, and the genera *Ca.* Nitrosopumilus and *Ca.* Nitrosopelagicus in all dives, and specifically the order Woesearchaeales in DiveC (Supplementary Tables S8–S10). *Ca.* Nitrosopelagicus (OTU1026) was mainly distributed in SS and nodule samples. OTUs from *Ca.* Nitrosopumilus were prevalent in OW and SS of all dives but abundant in nodules of DiveA and DiveC (Supplementary Tables S8–S10).

4 Discussion

4.1 Heterogeneous environments surrounding polymetallic nodules in the SCS

The South China Sea is hydrologically and geologically complex and is subject to a large terrestrial input and metal flux from continental shelf to the central deep-sea basin. It also experiences seasonal upwelling, high primary productivity, and a well-developed oxygen minimum zone (Guan et al., 2017; Zhong et al., 2017). Polymetallic nodules were mostly explored in the central basin of the SCS with low sedimentation rate (Zhong et al., 2017); however, in this study, we detected a wide and dense distribution of nodules in region A on the continental slope, with the morphology different from those collected from regions B and C (Figure 1B). It implied different formation mechanisms that could be affected by surrounding environments.

We found that POC flux from the upper water column and redox states in sediments were distinct among three regions, which could determine the scavenging of metals from seawater and porewater (Zhong et al., 2017). The quality and quantity of POC transported from the epipelagic layer to the deep ocean were key to determine the deep-sea sedimentary environments (Mestre et al., 2018). Although POC concentrations near the bottom of three stations were within the similar range (Figure 2C), the differences in POC sources could affect their fluxes and bioavailability in deep sea of three stations, potentially influencing the oxygen concentration and biogeochemical cycling. POC at Sta CTDB could be largely derived from terrestrial input (Figure 2C). The microbial composition and structure verified that SAR406 clade, SAR324 clade, and SAR202, which have been considered as free-living microbial groups adapted to oligotrophic environments (Boeuf et al., 2021; Geller-McGrath et al., 2023), were widely distributed below 200 m at Sta CTDB (Figure 3A). SAR406 clade and SAR202 clade indicated the refractory property of organic carbon at Sta CTDB because they were associated with the degradation of recalcitrant compounds (Thrash et al., 2017) and semi-labile alicyclic alkanes (Landry et al., 2017), respectively. SAR324 clade has been considered as particle-associated bacteria (PA) in epipelagic environment and FL in deep waters. The intense cluster of dominant SAR324 clade below 200 m (OTU1357) of Sta CTDB with deep-sea FL clades (Supplementary Figure S12) suggested that SAR324 clade were in FL mode and autotrophs (Swan et al., 2011; Boeuf et al., 2021). In contrast, nearly half of bathypelagic microbiome at stations CTDA and CTDC were dominated by PA lifestyle communities (Figure 3), including *Marinobacter* (23.8%) in the order Alteromonadales (Holtzapple and Schmidt-Dannert, 2007) and *Alcanivorax* (6.4-34.2%) and *Salinicola* (19.4-33.1%) in the order Oceanospirillales (Mason et al., 2012; Sebastián et al., 2021), all of which could rapidly utilize aliphatic hydrocarbons in the deep sea. In addition, higher proportions of *Oleibacter* in deep waters of stations CTDA and CTDC (Figure 3; Supplementary Table S2) indicated abundant aliphatic hydrocarbon (i.e., alkane; Liu et al., 2019). Thus, it implied that organic carbon could be more bioavailable in the deep sea of stations CTDA and CTDC, corresponding to the contribution of high proportion of phytoplankton-derived organic matter to total POC (Figure 2C). The relatively higher [NH_4^+] at the bottom of Sta CTDA (Supplementary Figure S3C) and rapid consumption of DO in the sediment core of DiveA (discussed below) indicated that organic carbon sinking to the deep water of Region A could be more abundant or labile.

The redox potential in the sediment core played a key role in mediating biogeochemical element cycling and manipulating deep-sea environment as a feedback (Zakem et al., 2020). Although our study did not directly measure or infer redox potential from geochemical parameters, we could use the microbial community in the sediment core as an index of the redox potential based on their well-established relationship (Wang et al., 2022) and the intense association of microbial and environmental properties in the water column of this study. The relative abundances of anaerobic microbial taxa, such as unidentified genera in orders Aminicenantales (Booker et al., 2023) and Marine Benthic Group A, the class Dehalococcoidia (Kaster et al., 2014; Yang et al., 2020), and the family Anaerolineae (Cai et al., 2021) of Chloroflexi, increased in sediment cores below 2 cm and 12 cm of DiveA and DiveB, respectively (Figures 4, 5). Aminicenantales dominated in anoxic ocean crust and were able to use organic carbon to drive sulfur oxides or extracellular iron oxyhydroxide reduction (Booker et al., 2023). Marine Benthic Group A was known to be found where nitrate was depleted (Durbin and Teske, 2011). It suggested a rapid depletion of oxygen and nitrate in top 2 cm of DiveA and 12 cm of DiveB. The relatively large numbers of two nitrifiers *Nitrospira* and Nitrosopumilaceae above the two layers could be active by receiving the substrate from nitrate reduction, since they have been detected

in anaerobic marine environment (Chen et al., 2017; Kraft et al., 2022; Martens-Habbena and Qin, 2022). Thus, the decrease in nitrifiers below the layers also suggested the depletion of nitrate (Figures 4, 5). The co-occurrence of Desulfobacterota and Lokiarchaeota observed at depths of 2–22 cm of DiveA and 12–22 cm of DiveB (Figure 5; Supplementary Figure S7) implied the initiation of sulfate reduction and iron oxide reduction, which were generally tightly linked (Jorgensen et al., 2012; Li et al., 2021). In the sediment core of DiveC, the increase in anaerobic groups from 4 cm (i.e., the class bacteriap25 of the phylum Myxococcota and the class DSEG of the phylum Aenigmarchaeota; Figure 4A; Cleary et al., 2023; Durbin and Teske, 2011) indicated the lack of oxygen starting at ~4 cm. DSEG was used to be detected before nitrate depletion (Durbin and Teske, 2011), suggesting enriched nitrate below 4 cm despite oxygen deficiency. The abundant Nitrosopumilaceae through the sediment core and consistent increase in *Nitrospira* from the surface layer likely revealed the supply of nitrate from nitrification process (Figures 4, 5; Hodgskiss et al., 2023; Garritano et al., 2023).

Overall, in terms of characteristics of microbial distribution and compositions in water columns and sediment cores of three regions, the geochemical environments at the bottom of the SCS were highly heterogeneous. As a consequence, the elemental fluxes, biogeochemical cycling, mineral precipitation, and geological features could be diverse and contributed to the alteration of redox conditions at interfaces of waters, sediments, and nodules, affecting the fate of elements involved in nodule formation.

4.2 Microbial interaction between polymetallic nodules and surrounding environments

The distinction of compositions and structures of the nodule communities from those in SS and OW in each region of the SCS (Figure 6; Supplementary Figures S8, S9) suggested that the nodule community was indigenous and not attributed to the simple accumulation from surrounding environments; however, the large discrepancy of microbial community in nodules among dives (Supplementary Figure S8) and the shared clusters with SS or OW in the corresponding dive (Figure 7; Supplementary Figures S9, S11; Supplementary Tables S5–S10) indicated the link of nodules and surrounding environments. Thus, the heterogeneous characteristics of deep-sea environments of three regions could eventually lead to the diversity in the formation of ferromanganese deposits in the SCS (Shulga et al., 2022).

The network based on bacterial communities in samples of DiveA showed an intense interaction between nodules (both NO and NI) and SS (Figure 7A; Supplementary Tables S4, S5). As discussed above, the deep sedimentary environment at DiveA likely received the most adequate supply of organic carbon among three regions. The high sedimentation rate and slow bottom current (monthly average < 1 cm/s; unpublished data) might create a stable and sub-oxic bottom environment for nodule growth, as indicated by the microbial composition in the sediment core. As discussed in *Section 4.1*, the activated reduction in Mn^{4+} and Fe^{3+} in shallow sediment layers could induce fluxes of Mn^{2+} and Fe^{2+} to the surface through the porewater (Hein et al., 2020; Shulga et al., 2022). The relatively abundant methanotrophs (i.e., Methyloligellaceae; Supplementary Figure S7; Knief, 2015) and methanogens (e.g., Methanofastidiosales; Figure 4A; Wang et al., 2021) present through the sediment core of DiveA, especially Methyloligeliaceae in SS, suggested that CH_4 oxidation could sustain sufficient reduced metals at the surface (González et al., 2012). Thus, the intense link between nodules and SS of DiveA in the network implied the sediment as the major sources of minerals for nodule formation in Region A. The families Magnetospiraceae, Kiloniellaceae, and Hyphomicrobiaceae associated with metal cycling were mostly shared by nodules and SS of DiveA, contributing significantly to the interaction between SS and nodules (Figure 6A; Supplementary Table S5). Hyphomicrobiaceae was functional in Mn oxidation (Tang et al., 2016), suggesting that the sediment-originated Mn was a major source to Fe–Mn deposits of DiveA. The NI shared most abundant OTUs with NO, SS, and OW at DiveA (Supplementary Figure S9), probably being caused by poor crystallization and a rapid growth of Mn-enriched nodules (Zhang C. et al., 2023). This was consistent with the characteristics of diagenetic Mn-enriched nodules in a stable growth environment (Zhong et al., 2017; Ren et al., 2023). The genus *Woeseia* and nitrifiers *Nitrospira*, *Nitrosomonas*, *AqS1* of Nitrosococcaceae, and Nitrosopumiliceae that had been enriched in Fe-rich deposit (Shulga et al., 2022) were abundant in SS and nodules, and the key groups in bacterial network of DiveA (Figure 6; Supplementary Table S5), implying the enrichment of Fe oxides in both niches. A more pronounced selection for Fe reducers (i.e., the family Magnetospiraceae; Matsunaga, 1991) in nodules and SS also reflected a higher content of an amorphous state of Fe minerals in a sub-oxic environment (Vereshchagin et al., 2019). Fe (i.e., pyrite, FeS_2) could originate from the upper water column through a large input of terrigenous materials in Region A (Figure 2C). We found a large number of symbiotic bacteria shared by SS and nodules, such as Kiloniellaceae and Subgroup21 (Schauer et al., 2010; Molari et al., 2020), which were associated with deep-sea benthic fauna (i.e., sponge, foraminifera; Cleary et al., 2023; Hori et al., 2013). It has been investigated that agglutinated foraminifera play a crucial role in nodule formation (Graham and Cooper, 1959; Greenslate, 1974). Thus, biological debris entrapped in nodules could be a mechanism of metal precipitation at DiveA (Molari et al., 2020; Wiese et al., 2020). Family Kiloniellaceae also owned potential of iron acquisition (Wang et al., 2015).

Different from DiveA, the microbial interaction between nodules and SS became weaker at DiveB and DiveC (Figures 7B, C; Supplementary Figures S11B, C; Supplementary Tables S6, S7, S9, S10), possibly a result of the variation in the redox state in sediments. The reduced metals might be oxidized before fluxing to the surface sediment (McKay et al., 2007). At DiveB, the bacterial network centrality was lowest among three regions and the archaeal one was lower than that of DiveA (Supplementary Table S4), suggesting the low association of nodules with surrounding environments in comparison to DiveA. Organic carbon was considered as refractory at DiveB due to much input of terrigenous components (Figure 2C); however, it could bring Fe-

rich waters to the deep ocean (Ziegler et al., 2008). The occurrence of large abundance of *Woeseia* again suggested enriched Fe in nodules (Figure 6A). Most of key bacterial OTUs in the network of DiveB belonged to SAR324 clade and SAR202 clade (Supplementary Table S6), which were abundant in nodule samples. It indicated that the nodule environment was in shortage of bioavailable carbon (see *Section 4.1*). SAR324 clade was also dominant in nodules from oligotrophic ocean, i.e., the South Pacific Gyre (Shiraishi et al., 2016) and the CCZ (Zhang C. et al., 2023). The accumulation of Fe deposit from upper water layers could be used as an energy source for autotrophic activity (Boeuf et al., 2021) or recalcitrant organic carbon degradation (Landry et al., 2017). SAR324 clade contained *nifH* gene encoding nitrogenase iron protein (Zhang D. et al., 2023), indicating the potential for N_2 fixation in nodules. It could provide nutrients for benthic organisms and enhance nitrogen cycling with enriched nitrifiers, i.e., *Nitrospira*, *Nitrospina*, *Ca.* Nitrosoplegicus, and family Nitrosopumilaceae (Figure 6). They all acquired iron as energy sources (Shafiee et al., 2021). The metal-cycling-related groups, such as families Kiloniellaceae and Hyphomicrobiaceae, did not share large numbers of OTUs among SS, OW, and nodules (Supplementary Table S6), suggesting that microbial mineralization was not the main process at interfaces of nodules. Family Magnetospiraceae (OTU1248) related to Fe cycle was mainly distributed in NI (Supplementary Table S6), revealing high contents of iron mineral in the nodule. The co-occurrence of sponge-associated bacteria Schekmanbacteria that were involved in sulfur cycling (Cleary et al., 2023) indicated the intense coupling of Fe–S cycling. Similarly, the order Puniceispirillales of SAR116 clade involved in Fe–S cycling was also detected ubiquitously in nodules of DiveB. They were mostly detected in eutrophic zone either in FL status or being associated with sponges or corals (Cleary et al., 2023; Roda-Garcia et al., 2023), implying that the nodule composition at DiveB (i.e., Fe) was affected by materials transported from the shallow waters. The detection of symbiotic bacteria also gave a hint that nodules collected at DiveB entrapped coral or sponge debris as the core of the nodule for subsequential formation. The decrease in shared OTUs between NI and other microbial niches (Supplementary Figure S9) and the distanced NI and NO in the networks (Figure 7B; Supplementary Figure S11B) revealed a large discrepancy of microbial community of NI from other environments. The nodule formation could be a long-term process, consistent with the record of slow growth of hydrogenetic nodules in the northwestern SCS (Zhong et al., 2017).

The highest bacterial network centrality of DiveC indicated an intense connectivity between nodules and surrounding environments (Figure 7C; Supplementary Table S4). SS and OW might co-affect the biogenic formation of nodules because they shared most bacterial or archaeal OTUs with NO (Supplementary Figure S9). It has been said the SCS nodules above the seamounts contained abundant hematite (Fe_2O_3) due to a narrowed oxygen minimum zone (OMZ; Zhong et al., 2019). A narrow OMZ was detected at Sta CTDC because the relatively high concentration of Chl-*a* could cause a rapid remineralization with a sharp consumption of oxygen at the mesopelagic zone (Figure 2D). Thus, the nodules at DiveC could be enriched with Fe oxides. Fe-scavenging family Magnetospiraceae was prevalent in both NI and NO (Matsunaga, 1991), confirming a high content and an amorphous state of Fe^{3+} minerals in nodules of DiveC (Vereshchagin et al., 2019; Ren et al., 2023). The presence of SAR324 clade in NO and NI indicated a low flux of organic carbon to the seafloor due to most degradation occurring in the

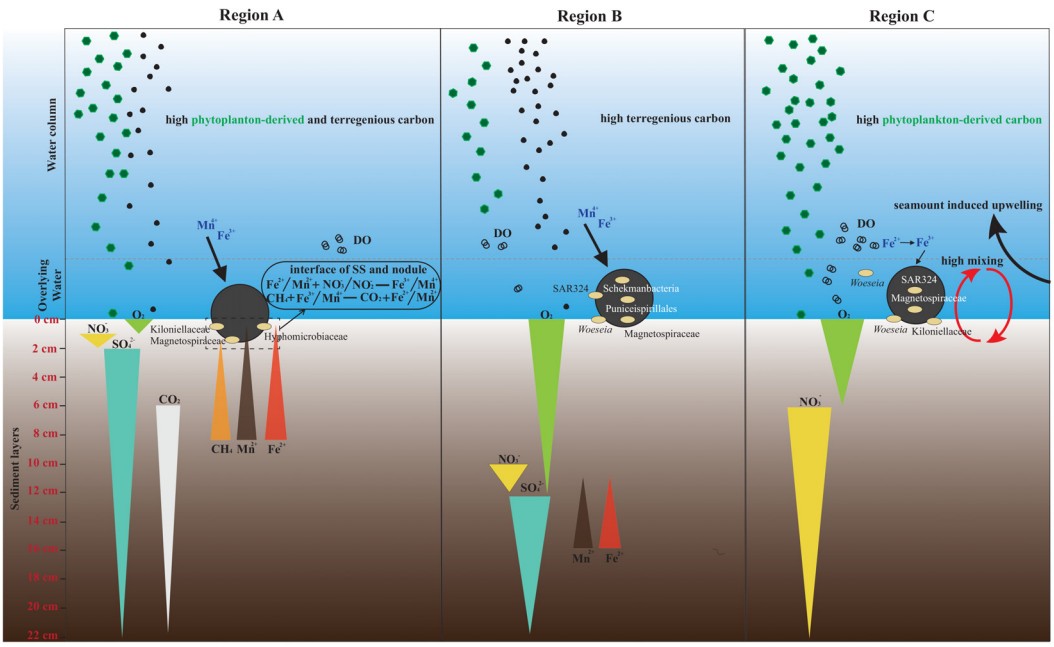

FIGURE 8
The hypothesized model of polymetallic nodule formation in three regions **(A–C)**. SS, surface sediment; DO, dissolved oxygen.

water column. The low Woesearchaeales and the high nitrifier (e.g., *Nitrospira* and Thaumarchaeota) abundances (Figure 6) suggested that NI was microaerobic, which could be a result of slow and loose formation under the condition of low sedimentation rate (Yang et al., 2024). The large divergence of microbial communities between NI and other three niches (Figure 6; Supplementary Figure S9) also suggested that the nodules were formed in a long process.

4.3 Potential mechanisms of polymetallic nodule formation

The nodule morphology at DiveA (Figure 1B) were similar to that collected in the northeastern SCS where the nodules were formed by early diagenesis and hydrogenetic growth according to the low Mn/Fe ratio and trace metal contents (Zhong et al., 2017). In our study, the hypothesized nodule formation at DiveA deduced from microbial compositions, functions in metal metabolisms, and microbial interactions between nodules and surrounding environments was consistent with previous results based on the analysis of elemental compositions. The shallow redox boundary (<2 cm) indicated by the microbial distribution in the sediment core reflected the sources of Fe–Mn deposits from the sediment, while a high input of terrigenous matter and relatively abundant Fe-utilizing microbes suggested the origin of Fe from seawaters (Figure 8). Although the nodules from DiveB and DiveC were inferred to be hydrogenetic, the source of metal ions could be different. At DiveB, the terrigenous matter fluxing into the deep-water could contribute to Fe–Mn deposits, and the debris of fauna from eutrophic zone of shelf waters or benthic environments enhanced the formation of nodules. At DiveC, the narrow OMZ induced by the intense degradation of phytoplankton-derived organic matter caused a low concentration of organic matter and rich oxygen in deep water, where Fe oxides were formed and enriched (Figure 8). Overall, relatively low sedimentation rates and strong bottom currents (monthly average < 3 cm/s and < 6 cm/s in regions B and C, respectively; unpublished data) induced by either coastal fluxes or upwelling and mixing at DiveB and DiveC could lead to a slow formation of the nodules.

5 Conclusion

In this study, we combined the investigations of hydrological properties and microbial communities of upper water columns, sediment cores, overlying waters, and polymetallic nodules for understanding the impact of environmental heterogeneity of the SCS on the formation of polymetallic nodules. In the water column, we found that the spatial variations of microbial communities and environmental characteristics in seawaters of three regions were consistent, suggesting that the distribution of microbial composition and diversity was a great indicator of the environment. The redox states in sediment cores inferred from microbial communities were diverse among three regions, potentially being affected by organic matter fluxes and physical dynamics in deep waters. The dissolved oxygen concentration in surface sediment of DiveA could be extremely low, which is beneficial for the overflow of reduced metals from the porewater for diagenetic formation of polymetallic nodules. Differently, polymetallic nodules at DiveB and DiveC, where bottom currents were relatively strong and sediments were more oxidized, could receive nodule constitutes from upper water layers (i.e., terrigenous-originated Fe at DiveB and Fe oxides from upper layer of seamount of DiveC). Overall, this study focused on microbe-mediated nodule formation process and provided a new perspective for understanding nodule formation mechanisms.

Data availability statement

The original contributions presented in the study are included in the article. Bacterial and archaeal 16S gene sequences have been deposited in the NCBI Sequence Read Archive under BioProject ID PRJNA1147917.

Author contributions

ML: Writing – review & editing, Writing – original draft, Visualization, Validation, Software, Methodology, Investigation, Formal analysis, Data curation. QL: Writing – review & editing, Writing – original draft, Visualization, Validation, Supervision, Software, Resources, Project administration, Methodology, Investigation, Funding acquisition, Formal analysis, Data curation, Conceptualization. XW: Writing – review & editing, Resources, Investigation, Data curation. DS: Writing – review & editing, Resources, Investigation, Data curation. LR: Writing – review & editing, Methodology, Investigation, Data curation. XL: Writing – review & editing, Investigation, Funding acquisition. CY: Writing – review & editing, Resources, Investigation, Data curation. BL: Writing – review & editing, Resources, Investigation. X-WX: Writing – review & editing, Supervision, Resources, Funding acquisition. C-SW: Writing – review & editing, Supervision, Project administration, Funding acquisition.

Funding

The author(s) declare financial support was received for the research, authorship, and/or publication of this article. This work was financially supported by the National Natural Science Foundation of China (no. 42176038), Scientific Research Fund of the Second Institute of Oceanography, MNR (no. SZ2401), the Project of State Key Laboratory of Satellite Ocean Environment Dynamics, Second Institute of Oceanography (no. SOEDZZ2204), and Science Foundation of Donghai Laboratory (no. DH-2022KF0211).

Conflict of interest

The authors declare that the research was conducted in the absence of any commercial or financial relationships that could be construed as a potential conflict of interest.

Publisher's note

Supplementary material

The Supplementary Material for this article can be found online at: https://www.frontiersin.org/articles/10.3389/fmars.2024.1430572/full#supplementary-material

SUPPLEMENTARY FIGURE 1
The images of polymetallic nodules on the seabed of DiveB in Region B and DiveC in Region C. The image was not successfully obtained by the camera mounted on the manned submersible 'Jiaolong' during DiveA in Region A.

SUPPLEMENTARY FIGURE 2
The rarefaction curves based on the Shannon index for the observed bacterial and archaeal OTUs from samples of **(A)** water columns and **(B)** sediment cores, nodules and overlying waters in all regions.

SUPPLEMENTARY FIGURE 3
Vertical distributions of **(A)** temperature, **(B)** salinity and **(C)** ammonium concentrations from 0-200 m (top row) and from 0-2000 m (bottom row).

SUPPLEMENTARY FIGURE 4
Shannon and Chao1 indices calculated for **(A)** bacterial and **(B)** archaeal communities in water column samples of stations CTDA, CTDB and CTDC, and **(C)** bacterial and **(D)** archaeal communities in sediment cores of DiveA, DiveB and DiveC in the South China Sea.

SUPPLEMENTARY FIGURE 5
Bacterial groups ranking 31-60 in the relative abundance in water column samples of stations CTDA, CTDB and CTDC in the South China Sea. The relative abundances of these groups were >0.01.

SUPPLEMENTARY FIGURE 6
β-diversity analysis of **(A)** bacterial and **(B)** archaeal communities in sediment cores of DiveA, DiveB and DiveC.

SUPPLEMENTARY FIGURE 7
Bacterial groups ranking 31-60 in the relative abundance in sediment cores of DiveA, DiveB and DiveC. The relative abundances of these groups were >0.01.

SUPPLEMENTARY FIGURE 8
(A) The comparisons of the means of **(A)** Shannon and **(B)** Chao1 indices of bacterial and archaeal communities of surface sediment (SS), overlying water (OW), nodule outside (NO) and nodule inside (NI) from all dives. $*p < 0.05$, $** p < 0.01$, $*** p < 0.001$. **(C)** ANOSIM analysis for bacterial and archaeal communities of SS, OW, NO and NI from all dives. The boxes of 'SS', 'OW', 'NO' and 'NI' represented the distance values within samples of the same sample type. The boxes of 'Between' represented the distance values between all samples.

SUPPLEMENTARY FIGURE 9
Venn analysis on OTU level. The numbers and the proportions of the common **(A)** bacterial OTUs or **(B)** archaeal OTUs shared by surface sediments (SS), overlying waters (OW) and nodules (NO, nodule outside; NI, nodule inside) were shown for DiveA, DiveB and DiveC.

SUPPLEMENTARY FIGURE 10
Bacterial groups ranking 31-60 in the relative abundance in surface sediments (SS), overlying waters (OW), nodules (NO, nodule outside; NI, nodule inside) of DiveA, DiveB and DiveC. The relative abundances of these groups were >0.01.

SUPPLEMENTARY FIGURE 11
Collinear network analysis at archaeal OTU level on samples of surface sediment (SS), overlying water (OW) and nodules (NO, nodule outside; NI, nodule inside) for **(A)** DiveA, **(B)** DiveB and **(C)** DiveC. Networks were analyzed based on all OTUs of each dive, but only those with the number beyond 200 were displayed.

SUPPLEMENTARY FIGURE 12
Maximum Likelihood phylogenetic tree was constructed for SAR324 OTUs obtained from water column samples of stations CTDA, CTDB and CTDC. The reference sequences were obtained by NCBI 'blast' alignment. The pie charts showed the distribution of OTUs at different water depths.

References

Anderson, M. J. (2006). Distance-based tests for homogeneity of multivariate dispersions. *Biometrics* 62, 245–253. doi: 10.1111/j.1541-0420.2005.00440.x

Blöthe, M., Wegorzewski, A., Müller, C., Simon, F., Kuhn, T., and Schippers, A. (2015). Manganese-cycling microbial communities inside deep-sea manganese nodules. *Environ. Sci. Technol.* 49, 7692–7700. doi: 10.1021/es504930v

Boeuf, D., Eppley, J. M., Mende, D. R., Malmstrom, R. R., Woyke, T., and DeLong, E. F. (2021). Metapangenomics reveals depth-dependent shifts in metabolic potential for the ubiquitous marine bacterial SAR324 lineage. *Microbiome* 9, 172. doi: 10.1186/s40168-021-01119-5

Bolger, A. M., Lohse, M., and Usadel, B. (2014). Trimmomatic: a flexible trimmer for Illumina sequence data. *Bioinformatics* 30, 2114–2120. doi: 10.1093/bioinformatics/btu170

Booker, A. E., D'Angelo, T., Adams-Beyea, A., Brown, J. M., Nigro, O., Rappé, M. S., et al. (2023). Life strategies for *Aminicenantia* in subseafloor oceanic crust. *ISME J.* 17, 1406–1415. doi: 10.1038/s41396-023-01454-5

Bröhl, T., and Lehnertz, K. (2022). A straightforward edge centrality concept derived from generalizing degree and strength. *Sci. Rep.* 12, 4407. doi: 10.1038/s41598-022-08254-5

Cai, C., Li, L., Hua, Y., Liu, H., and Dai, X. (2021). Ferroferric oxide promotes metabolism in Anaerolineae other than microbial syntrophy in anaerobic methanogenesis of antibiotic fermentation residue. *Sci. Total Environ.* 758, 143601. doi: 10.1016/j.scitotenv.2020.143601

Caporaso, J. G., Lauber, C. L., Walters, W. A., Berg-Lyons, D., Lozupone, C. A., Turnbaugh, P. J., et al. (2011). Global patterns of 16S rRNA diversity at a depth of millions of sequences per sample. *Proc. Natl. Acad. Sci. U.S.A.* 108, 4516–4522. doi: 10.1073/pnas.1000080107

Chen, C., Chen, H., Zhang, Y., Thomas, H. R., Frank, M. H., He, Y., et al. (2020). TBtools: an integrative toolkit developed for interactive analyses of big biological data. *Mol. Plant* 13, 1194–1202. doi: 10.1016/j.molp.2020.06.009

Chen, S., Yin, X., Wang, X., Huang, X., Ma, Y., Guo, K., et al. (2018). The geochemistry and formation of ferromanganese oxides on the eastern flank of the Gagua Ridge. *Ore Geology Rev.* 95, 118–130. doi: 10.1016/j.oregeorev.2018.02.026

Chen, Y., Liu, Y., and Wang, X. (2017). Spatiotemporal variation of bacterial and archaeal communities in sediments of a drinking reservoir, Beijing, China. *Appl. Microbiol. Biotechnol.* 101, 3379–3391. doi: 10.1007/s00253-016-8019-1

Clarke, K., and Gorley, R. N. (2006). *Primer v6: user manual/tutorial* (Plymouth: PRIMER-E).

Cleary, D. F. R., Oliveira, V., Gomes, N. C. M., Bialecki, A., and de Voogd, N. J. (2023). A comparison of free-living and sponge-associated bacterial communities from

a remote oceanic island with a focus on calcareous sponges. *FEMS Microbiol. Ecol.* 99, fiad014. doi: 10.1093/femsec/fiad014

Durbin, A. M., and Teske, A. (2011). Microbial diversity and stratification of South Pacific abyssal marine sediments. *Environ. Microbiol.* 13, 3219–3234. doi: 10.1111/j.1462-2920.2011.02544.x

Edgar, R. C. (2013). UPARSE: highly accurate OTU sequences from microbial amplicon reads. *Nat. Methods* 10, 996–998. doi: 10.1038/nmeth.2604

Ehrlich, H. L. (1963). Bacteriology of manganese nodules: I. Bacterial action on manganese in nodule enrichments. *Appl. Microbiol.* 11, 15–19. doi: 10.1128/am.11.1.15-19.1963

Garritano, A. N., Majzoub, M. E., Ribeiro, B., Damasceno, T., Modolon, F., Messias, C., et al. (2023). Species-specific relationships between deep sea sponges and their symbiotic *Nitrosopumilaceae*. *ISME J.* 17, 1517–1519. doi: 10.1038/s41396-023-01439-4

Geller-McGrath, D., Mara, P., Taylor, G. T., Suter, E., Edgcomb, V., and Pachiadaki, M. (2023). Diverse secondary metabolites are expressed in particle-associated and free-living microorganisms of the permanently anoxic Cariaco Basin. *Nat. Commun.* 14, 656. doi: 10.1038/s41467-023-36026-w

González, F. J., Somoza, L., Hein, J. R., Medialdea, T., León, R., Urgorri, V., et al. (2016). Phosphorites, Co-rich Mn nodules, and Fe-Mn crusts from Galicia Bank, NE Atlantic: Reflections of Cenozoic tectonics and paleoceanography: MINERALIZATIONS FROM GALICIA BANK. *Geochem. Geophys. Geosyst.* 17, 346–374. doi: 10.1002/2015GC005861

González, F. J., Somoza, L., León, R., Medialdea, T., de Torres, T., Ortiz, J. E., et al. (2012). Ferromanganese nodules and micro-hardgrounds associated with the Cadiz Contourite Channel (NE Atlantic): Palaeoenvironmental records of fluid venting and bottom currents. *Chem. Geology* 310–311, 56–78. doi: 10.1016/j.chemgeo.2012.03.030

Graham, J. W., and Cooper, S. C. (1959). Biological origin of manganese-rich deposits of the sea floor. *Nature* 183, 1050–1051. doi: 10.1038/1831050a0

Greenslate, J. (1974). Microorganisms participate in the construction of manganese nodules. *Nature* 249, 181–183. doi: 10.1038/249181a0

Guan, Y., Ren, Y., Sun, X., Xiao, Z., Wu, Z., Liao, J., et al. (2019). Fine scale study of major and trace elements in the Fe-Mn nodules from the South China Sea and their metallogenic constraints. *Mar. Geology* 416, 105978. doi: 10.1016/j.margeo.2019.105978

Guan, Y., Sun, X., Ren, Y., and Jiang, X. (2017). Mineralogy, geochemistry and genesis of the polymetallic crusts and nodules from the South China Sea. *Ore Geology Rev.* 89, 206–227. doi: 10.1016/j.oregeorev.2017.06.020

Hang, W., and Wang, P. (2006). Sediment mass and distribution in the south china sea since the oligocene. *Sci. China Ser. D Earth Sci.* 49, 1147–1155.

Hagberg, A. A., Schult, D. A., and Swart, P. J. (2008). "Exploring network structure, dynamics, and function using NetworkX," in Gäel Varoquaux, Travis Vaught and Jarrod Millman (Eds). *Proceeding of the 7th Python in Science Conference (SciPy2008)*, 11–15 (Pasadena, CA USA).

Halbach, P., Hebisch, U., and Scherhag, C. (1981). Geochemical variations of ferromanganese nodules and crusts from different provinces of the Pacific Ocean and their genetic control. *Chem. Geology* 34, 3–17. doi: 10.1016/0009-2541(81)90067-X

Hein, J. R., and Koschinsky, A. (2014). *Deep-ocean ferromanganese crusts and nodules, in: treatise on geochemistry* (Amsterdam: Elsevier), 273–291. doi: 10.1016/B978-0-08-095975-7.01111-6

Hein, J. R., Koschinsky, A., and Kuhn, T. (2020). Deep-ocean polymetallic nodules as a resource for critical materials. *Nat. Rev. Earth Environ.* 1, 158–169. doi: 10.1038/s43017-020-0027-0

Hein, J. R., Koschinsky, A., and McIntyre, B. R. (2005). Mercury- and silver-rich ferromanganese oxides, southern california borderland: deposit model and environmental implications. *Economic Geology* 100, 1151–1168. doi: 10.2113/gsecongeo.100.6.1151

Hein, J. R., Mizell, K., Koschinsky, A., and Conrad, T. A. (2013). Deep-ocean mineral deposits as a source of critical metals for high- and green-technology applications: Comparison with land-based resources. *Ore Geology Rev.* 51, 1–14. doi: 10.1016/j.oregeorev.2012.12.001

Hein, J. R., Spinardi, F., Okamoto, N., Mizell, K., Thorburn, D., and Tawake, A. (2015). Critical metals in manganese nodules from the Cook Islands EEZ, abundances and distributions. *Ore Geology Rev.* 68, 97–116. doi: 10.1016/j.oregeorev.2014.12.011

Hodgskiss, L. H., Melcher, M., Kerou, M., Chen, W., Ponce-Toledo, R. I., Savvides, S. N., et al. (2023). Unexpected complexity of the ammonia monooxygenase in archaea. *ISME J.* 17, 588–599. doi: 10.1038/s41396-023-01367-3

Hollingsworth, A. L., Jones, D. O. B., and Young, C. R. (2021). Spatial variability of abyssal nitrifying microbes in the north-eastern clarion-clipperton zone. *Front. Mar. Sci.* 8. doi: 10.3389/fmars.2021.663420

Holtzapple, E., and Schmidt-Dannert, C. (2007). Biosynthesis of isoprenoid wax ester in marinobacter hydrocarbonoclasticus DSM 8798: identification and characterization of isoprenoid coenzyme A synthetase and wax ester synthases. *J. Bacteriol* 189, 3804–3812. doi: 10.1128/JB.01932-06

Hori, S., Tsuchiya, M., Nishi, S., Arai, W., Yoshida, T., and Takami, H. (2013). Active bacterial flora surrounding foraminifera (Xenophyophorea) living on the deep-sea floor. *Bioscience Biotechnology Biochem.* 77, 381–384. doi: 10.1271/bbb.120663

Jiang, X. D., Zhao, X., Chou, Y. M., Liu, Q. S., Roberts, A. P., Ren, J. B., et al. (2020). Characterization and quantification of magnetofossils within abyssal manganese nodules from the western pacific ocean and implications for nodule formation. *Geochem. Geophys. Geosyst* 21. doi: 10.1029/2019GC008811

Kaster, A., Mayer-Blackwell, K., Pasarelli, B., and Spormann, A. M. (2014). Single cell genomic study of Dehalococcoidetes species from deep-sea sediments of the Peruvian margin. *ISME J.* 8, 1831–1842.

Jorgensen, S. L., Hannisdal, B., Lanzen, A., Baumberger, T., Flesland, K., Fonseca, R., et al. (2012). Correlating microbial community profiles with geochemical data in highly stratified sediments from the arctic mid-ocean ridge. *Proc. Nalt. Acad. Sci. U. S. A.* 109, 16764–16765.

Knief, C. (2015). Diversity and habitat preferences of cultivated and uncultivated aerobic methanotrophic bacteria evaluated based on pmoA as molecular marker. *Front. Microbiol.* 6. doi: 10.3389/fmicb.2015.01346

Kraft, B., Jehmlich, N., Larsen, M., Bristow, L. A., Könneke, M., Thamdrup, B., et al. (2022). Oxygen and nitrogen production by an ammonia-oxidizing archaeon. *Science* 375, 97–100. doi: 10.1126/science.abe6733

Kronthaler, F., and Zöllner, S. (2021). *R and RStudio, in: data analysis with RStudio* (Berlin, Heidelberg: Springer Berlin Heidelberg), 1–12. doi: 10.1007/978-3-662-62518-7_1

Kuhn, T., Wegorzewski, A., Rühlemann, C., and Vink, A. (2018). Correction to: composition, formation, and occurrence of polymetallic nodules, Chapter 2 in *Deep-Sea Mining*, R. Sharma (ed.). Springer International Publishing, Cham). doi: 10.1007/978-3-319-52557-0_19

Landry, Z., Swan, B. K., Herndl, G. J., Stepanauskas, R., and Giovannoni, S. J. (2017). SAR202 genomes from the dark ocean predict pathways for the oxidation of recalcitrant dissolved organic matter. *mBio* 8, e00413–e00417. doi: 10.1128/mBio.00413-17

Li, J., Li, L., Bai, S., Chen, S., Xu, H., Ta, K., et al. (2021). Geochemical and molecular characteristics of ferromanganese deposits and surrounding sediments in the Mariana Trench: An Implication for the geochemical Mn cycle in sedimentary environments of the trench zone. *Geochimica Cosmochimica Acta* 310, 155–168. doi: 10.1016/j.gca.2021.07.018

Lindh, M. V., Maillot, B. M., Shulse, C. N., Gooday, A. J., Amon, D. J., Smith, C. R., et al. (2017). From the surface to the deep-sea: bacterial distributions across polymetallic nodule fields in the clarion-clipperton zone of the pacific ocean. *Front. Microbiol.* 8. doi: 10.3389/fmicb.2017.01696

Liu, J., Huang, F., Liu, J., Liu, X., Lin, R., Zhong, X., et al. (2023). Phylotype resolved spatial variation and association patterns of planktonic Thaumarchaeota in eastern Chinese marginal seas. *Mar. Life Sci. Technol.* 5, 257–270. doi: 10.1007/s42995-023-00169-y

Liu, J., Zheng, Y., Lin, H., Wang, X., Li, M., Liu, Y., et al. (2019). Proliferation of hydrocarbon-degrading microbes at the bottom of the Mariana Trench. *Microbiome* 7, 47. doi: 10.1186/s40168-019-0652-3

Liu, J., Zhu, S., Liu, X., Yao, P., Ge, T., and Zhang, X.-H. (2020). Spatiotemporal dynamics of the archaeal community in coastal sediments: assembly process and co-occurrence relationship. *ISME J.* 14, 1463–1478. doi: 10.1038/s41396-020-0621-7

Marino, E., González, F. J., Somoza, L., Lunar, R., Ortega, L., Vázquez, J. T., et al. (2017). Strategic and rare elements in Cretaceous-Cenozoic cobalt-rich ferromanganese crusts from seamounts in the Canary Island Seamount Province (northeastern tropical Atlantic). *Ore Geology Rev.* 87, 41–61. doi: 10.1016/j.oregeorev.2016.10.005

Martens-Habbena, W., and Qin, W. (2022). Archaeal nitrification without oxygen. *Science* 375, 27–28. doi: 10.1126/science.abn0373

Mason, O. U., Hazen, T. C., Borglin, S., Chain, P. S. G., Dubinsky, E. A., Fortney, J. L., et al. (2012). Metagenome, metatranscriptome and single-cell sequencing reveal microbial response to Deepwater Horizon oil spill. *ISME J.* 6, 1715–1727. doi: 10.1038/ismej.2012.59

Matsunaga, T., Sakaguchi, T., and Tadakoro, F. (1991). Magnetite formation by a magnetic bacterium capable of growing aerobically. *Appl. Microb. Biotechnol.* 35, 651–655.

McKay, J. L., Pedersen, T. F., and Mucci, A. (2007). Sedimentary redox conditions in continental margin sediments (N.E. Pacific)—Influence on the accumulation of redox-sensitive trace metals. *Chem. Geology* 238, 180–196. doi: 10.1016/j.chemgeo.2006.11.008

Mestre, M., Ruiz-González, C., Logares, R., Duarte, C. M., Gasol, J. M., and Sala, M. M. (2018). Sinking particles promote vertical connectivity in the ocean microbiome. *Proc. Natl. Acad. Sci. U.S.A.* 115, E6799–E6807. doi: 10.1073/pnas.1802470115

Molari, M., Janssen, F., Vonnahme, T. R., Wenzhöfer, F., and Boetius, A. (2020). The contribution of microbial communities in polymetallic nodules to the diversity of the deep-sea microbiome of the Peru Basin (4130–4198 m depth). *Biogeosciences* 17, 3203–3222. doi: 10.5194/bg-17-3203-2020

Ren, Y., Guan, Y., Sun, X., Xu, L., Xiao, Z., Deng, Y., et al. (2023). Nano-mineralogy and growth environment of Fe-Mn polymetallic crusts and nodules from the South China Sea. *Front. Mar. Sci.* 10. doi: 10.3389/fmars.2023.1141926

Roda-Garcia, J. J., Haro-Moreno, J. M., and López-Pérez, M. (2023). Evolutionary pathways for deep-sea adaptation in marine planktonic Actinobacteriota. *Front. Microbiol.* 14. doi: 10.3389/fmicb.2023.1159270

Schauer, R., Bienhold, C., Ramette, A., and Harder, J. (2010). Bacterial diversity and biogeography in deep-sea surface sediments of the South Atlantic Ocean. *ISME J.* 4, 159–170. doi: 10.1038/ismej.2009.106

Sebastián, M., Sánchez, P., Salazar, G., Álvarez-Salgado, X. A., Reche, I., Morán, X. A. G., et al. (2021). The quality of dissolved organic matter shapes the biogeography of the active bathypelagic microbiome. *bioRxiv*. [preprint]. doi: 10.1101/2021.05.14.444136

Shafiee, R. T., Diver, P. J., Snow, J. T., Zhang, Q., and Rickaby, R. E. M. (2021). Marine ammonia-oxidising archaea and bacteria occupy distinct iron and copper niches. *ISME Commun.* 1, 1. doi: 10.1038/s43705-021-00001-7

Shannon, P., Markiel, A., Ozier, O., Baliga, N. S., Wang, J. T., Ramage, D., et al. (2003). Cytoscape: a software environment for integrated models of biomolecular interaction networks. *Genome Res*. 13, 2498–2504.

Sheik, C. S., Reese, B. K., Twing, K. I., Sylvan, J. B., Grim, S. L., Schrenk, M. O., et al. (2018). Identification and removal of contaminant sequences from ribosomal gene databases: lessons from the census of deep life. *Front. Microbiol.* 9. doi: 10.3389/fmicb.2018.00840

Shiraishi, F., Mitsunobu, S., Suzuki, K., Hoshino, T., Morono, Y., and Inagaki, F. (2016). Dense microbial community on a ferromanganese nodule from the ultra-oligotrophic South Pacific Gyre: Implications for biogeochemical cycles. *Earth Planetary Sci. Lett.* 447, 10–20. doi: 10.1016/j.epsl.2016.04.021

Shulga, N., Abramov, S., Klyukina, A., Ryazantsev, K., and Gavrilov, S. (2022). Fast-growing Arctic Fe–Mn deposits from the Kara Sea as the refuges for cosmopolitan marine microorganisms. *Sci. Rep.* 12, 21967. doi: 10.1038/s41598-022-23449-6

Shulse, C. N., Maillot, B., Smith, C. R., and Church, M. J. (2017). Polymetallic nodules, sediments, and deep waters in the equatorial North Pacific exhibit highly diverse and distinct bacterial, archaeal, and microeukaryotic communities. *MicrobiologyOpen* 6, e00428. doi: 10.1002/mbo3.428

Swan, B. K., Martinez-Garcia, M., Preston, C. M., Sczyrba, A., Woyke, T., Lamy, D., et al. (2011). Potential for chemolithoautotrophy among ubiquitous bacteria lineages in the dark ocean. *Science* 333, 1296–1300. doi: 10.1126/science.1203690

Tang, W., Gong, J., Wu, L., Li, Y., Zhang, M., and Zeng, X. (2016). DGGE diversity of manganese mine samples and isolation of a Lysinibacillus sp. efficient in removal of high Mn (II) concentrations. *Chemosphere* 165, 277–283. doi: 10.1016/j.chemosphere.2016.08.134

Thrash, J. C., Seitz, K. W., Baker, B. J., Temperton, B., Gillies, L. E., Rabalais, N. N., et al. (2017). Metabolic roles of uncultivated bacterioplankton lineages in the northern gulf of Mexico "Dead zone. *mBio* 8, e01017–e01017. doi: 10.1128/mBio.01017-17

Tully, B. J., and Heidelberg, J. F. (2013). Microbial communities associated with ferromanganese nodules and the surrounding sediments. *Front. Microbiol.* 4. doi: 10.3389/fmicb.2013.00161

Vereshchagin, O. S., Perova, E. N., Brusnitsyn, A. I., Ershova, V. B., Khudoley, A. K., Shilovskikh, V. V., et al. (2019). Ferro-manganese nodules from the Kara Sea: Mineralogy, geochemistry and genesis. *Ore Geology Rev.* 106, 192–204. doi: 10.1016/j.oregeorev.2019.01.023

von Stackelberg, U. (1997). Growth history of manganese nodules and crusts of the Peru Basin. *SP* 119, 153–176. doi: 10.1144/GSL.SP.1997.119.01.11

von Stackelberg, U. (2017). "Manganese nodules of the Peru basin," in *Handbook of marine mineral deposits*. Ed. D. S. Cronan (New York: Routledge), 197–238. doi: 10.1201/9780203752760-8

Wang, L., Li, X., Lai, Q., and Shao, Z. (2015). Kiloniella litopenaei sp. nov., isolated from the gut microflora of Pacific white shrimp, Litopenaeus vannamei. *Antonie van Leeuwenhoek* 108, 1293–1299. doi: 10.1007/s10482-015-0581-5

Wang, Y., Wegener, G., Williams, T. A., Xie, R., Hou, J., Tian, C., et al. (2021). A methylotrophic origin of methanogenesis and early divergence of anaerobic multicarbon alkane metabolism. *Sci. Adv.* 7, eabj1453. doi: 10.1126/sciadv.abj1453

Wang, Z., Liu, F., Li, E., Yuan, Y., Yang, Y., Xu, M., et al. (2022). Network analysis reveals microbe-mediated impacts of aeration on deep sediment layer microbial communities. *Front. Microbiol.* 13. doi: 10.3389/fmicb.2022.931585

Wasserman, S., and Faust, K. (1994). *Social network analysis: methods and applications, 1st ed* (Cambridge: Cambridge University Press). doi: 10.1017/CBO9780511815478

Wiese, J., Imhoff, J. F., Horn, H., Borchert, E., Kyrpides, N. C., Göker, M., et al. (2020). Genome analysis of the marine bacterium Kiloniella laminariae and first insights into comparative genomics with related Kiloniella species. *Arch. Microbiol.* 202, 815–824. doi: 10.1007/s00203-019-01791-0

Wu, Y.-H., Liao, L., Wang, C.-S., Ma, W.-L., Meng, F.-X., Wu, M., et al. (2013). A comparison of microbial communities in deep-sea polymetallic nodules and the surrounding sediments in the Pacific Ocean. *Deep Sea Res. Part I: Oceanographic Res. Papers* 79, 40–49. doi: 10.1016/j.dsr.2013.05.004

Yang, K., Dong, Y., Li, Z., Wang, H., Ma, W., Qiu, Z., et al. (2024). Geochemistry of buried polymetallic nodules from the eastern Pacific Ocean: Implication for the depth-controlled alteration process. *Mar. Geology* 467, 107190. doi: 10.1016/j.margeo.2023.107190

Yang, Y., Sanford, R., Yan, J., Chen, G., Cápiro, N. L., Li, X., et al. (2020). Roles of organohalide-respiring dehalococcoidia in carbon cycling. *mSystems* 5, e00757–e00719. doi: 10.1128/mSystems.00757-19

Yuan, Y. C., Rickard, L. N., Xia, L., and Scherer, C. (2011). The interplay between interpersonal and electronic resources in knowledge seeking among co-located and distributed employees. *J. Am. Soc Inf. Sci.* 62, 535–549. doi: 10.1002/asi.21472

Zakem, E. J., Polz, M. F., and Follows, M. J. (2020). Redox-informed models of global biogeochemical cycles. *Nat. Commun.* 11, 5680. doi: 10.1038/s41467-020-19454-w

Zhang, C., Liu, X., Shi, L.-D., Li, J., Xiao, X., Shao, Z., et al. (2023). Unexpected genetic and microbial diversity for arsenic cycling in deep sea cold seep sediments. *NPJ Biofilms Microbiomes* 9, 13. doi: 10.1038/s41522-023-00382-8

Zhang, D., Li, X., Wu, Y., Xu, X., Liu, Y., Shi, B., et al. (2023). Microbe-driven elemental cycling enables microbial adaptation to deep-sea ferromanganese nodule sediment fields. *Microbiome* 11, 160. doi: 10.1186/s40168-023-01601-2

Zhang, Z., Du, Y., Wu, C., Fang, N., Yang, S., Liu, J., et al. (2013). Growth of a polymetallic nodule from the northwestern continental margin of the South China Sea and its response to changes in the paleoceanographical environment of the Late Cenozoic. *Sci. China Earth Sci.* 56, 453–463. doi: 10.1007/s11430-012-4535-8

Zheng, X., Su, Y., Li, X., Xiao, N., Wang, D., and Chen, Y. (2013). Pyrosequencing reveals the key microorganisms involved in sludge alkaline fermentation for efficient short-chain fatty acids production. *Environ. Sci. Technol.* 47, 4262–4268. doi: 10.1021/es400210v

Zhong, Y., Chen, Z., González, F. J., Hein, J. R., Zheng, X., Li, G., et al. (2017). Composition and genesis of ferromanganese deposits from the northern South China Sea. *J. Asian Earth Sci.* 138, 110–128. doi: 10.1016/j.jseaes.2017.02.015

Zhong, Y., Chen, Z., Hein, J. R., González, F. J., Jiang, Z., Yang, X., et al. (2020). Evolution of a deep-water ferromanganese nodule in the South China Sea in response to Pacific deep-water circulation and continental weathering during the Plio-Pleistocene. *Quaternary Sci. Rev.* 229, 106106. doi: 10.1016/j.quascirev.2019.106106

Zhong, Y., Liu, Q., Chen, Z., González, F. J., Hein, J. R., Zhang, J., et al. (2019). Tectonic and paleoceanographic conditions during the formation of ferromanganese nodules from the northern South China Sea based on the high-resolution geochemistry, mineralogy and isotopes. *Mar. Geology* 410, 146–163. doi: 10.1016/j.margeo.2018.12.006

Ziegler, C. L., Murray, R. W., Plank, T., and Hemming, S. R. (2008). Sources of fe to the equatorial pacific ocean from the holocene to miocene. *Earth Planetary Sci. Lett.* 270, 258–270. doi: 10.1016/j.epsl.2008.03.044